

Chapter 9

COMPARATIVE CRYSTAL CHEMISTRY OF DENSE OXIDE MINERALS

Joseph R. Smyth, Steven D. Jacobsen

*Department of Geological Sciences, 2200 Colorado Avenue,
University of Colorado, Boulder, CO 80309-0399
and*

*Bayerisches Geoinstitut, Universität Bayreuth
D95440 Bayreuth, Germany*

Robert M. Hazen

*Geophysical Laboratory, 5251 Broad Branch Road NW,
Washington, DC 20015-1305*

INTRODUCTION

Oxygen is the most abundant element in the Earth, constituting about 43 percent by weight of the crust and mantle. While most of this mass is incorporated into silicates, the next most abundant mineral group in the planet is the oxides. The oxide minerals are generally considered to be those oxygen-based minerals that do not contain a distinct polyanionic species such as OH^- , CO_3^{2-} , SO_4^{2-} , PO_4^{3-} , SiO_4^{4-} , etc. The oxide structures are also of interest in mineral physics, because, at high pressure, many silicates are known to adopt structures similar to the dense oxides (see Hazen and Finger *this volume*).

Oxide minerals, because of their compositional diversity and structural simplicity, have played a special role in the development of comparative crystal chemistry. Many of the systematic empirical relationships regarding the behavior of structures with changing temperature and pressure were first defined and illustrated with examples drawn from these phases. Oxides thus provide a standard for describing and interpreting the behavior of more complex compounds. Our principal objectives here are to review the mineral structures that have been studied at elevated temperatures and pressures, to compile thermal expansion and compression data for the various structural elements in a consistent fashion, and to explore systematic aspects of their structural behavior at nonambient conditions. The large and growing number of single-crystal structure investigations of the simpler or more important dense oxides at high pressures and temperatures warrant this comparative synthesis.

Regarding thermal expansion for various structural elements, we have chosen to assume linear expansion coefficients. This approach facilitates comparison across disparate structures and methodologies, and it reflects the reality that data are not sufficiently precise in many cases to permit the meaningful derivation of second-order thermal expansion parameters. For compression data we have also computed linear axial compressibilities to facilitate comparison of the various axes, but we have retained the pressure derivative of the bulk modulus, K' , where refined or assumed the standard value of 4 for K' .

The scope of this chapter is dictated by the range of naturally-occurring oxide structure types. Oxide minerals may be divided conveniently into the simple oxides, which contain a single cationic site or species, and the binary oxides, which contain two distinct cationic sites or species. The alkali elements do not occur as simple oxide minerals, so the only natural X_2O mineral, other than ice (see Chapter 15 by Hemley and Dera in this volume), is cuprite (Cu_2O). No structural studies have yet been undertaken on cuprite at non-ambient conditions.

In contrast to the simple oxides of monovalent cations, many oxide minerals of divalent cations are known, and several of these are of major geophysical significance. Of these minerals, the periclase group with the rocksalt (NaCl) structure are the most widely studied at non-ambient conditions. The periclase-wüstite [(Mg,Fe)O] solid solution is likely to be a major constituent of the lower mantle. In addition, the periclase group includes lime (CaO), manganosite (MnO), bunsenite (NiO), monteponite (CdO) and hongquite (TiO), as well as synthetic alkaline earth and rare-earth oxides. Other monoxides include bromellite (BeO) and zincite (ZnO), which have the wurtzite structure, tenorite (CuO), litharge ($\alpha\text{-PbO}$), massicot ($\beta\text{-PbO}$), romarchite (SnO) and montroydite (HgO). Of these minerals, only bromellite, litharge, and massicot have been studied at pressure.

The sesquioxide minerals include oxides of trivalent cations. The most important sesquioxide minerals are in the corundum group, which includes corundum (Al_2O_3), hematite (Fe_2O_3), eskolaite (Cr_2O_3) and karelianite (V_2O_3), as

well as Ti_2O_3 . The structures of all five of these have been investigated at temperature and pressure. Other sesquioxide minerals, none of whose structures have been studied at non-ambient conditions, include bixbyite (Mn_2O_3), which is isostructural with avicennite (Tl_2O_3) and several of the rare earth oxides, and some minor oxides of chalcophile metals, such as s enarmontite and valentinite (Sb_2O_3), arsenolite and claudetite (As_2O_3), and bismite (Bi_2O_3).

The dioxide minerals include the oxides of tetravalent cations. The large and important rutile group includes rutile (TiO_2), stishovite (SiO_2), cassiterite (SnO_2) and pyrolusite (MnO_2), as well as several synthetic isomorphs. In addition to rutile, TiO_2 polymorphs include anatase and brookite, as well as the high-pressure forms with the baddeleyite and $\alpha\text{-PbO}_2$ structures. Other dioxides include the mineral baddeleyite (ZrO_2), and the uraninite group, including the fluorite-structure minerals, cerianite (CeO_2), uraninite (UO_2), and thorianite (ThO_2).

In addition to these simple oxide minerals, numerous binary oxides are known with two different cations in at least two distinct crystallographic sites. Major binary oxide groups considered in this volume include the ilmenite and perovskite groups (ABO_3), the spinel and spinelloid groups (AB_2O_4), the pseudobrookite group (A_2BO_5), and the scheelite group (ABO_4).

SIMPLE OXIDES

Cuprite group (A_2O)

The alkali elements do not occur as simple oxide minerals, because their large ionic radii typically require coordination numbers of six or greater. Six-coordination of an alkali cation by oxygen would necessitate an unrealistic twelve-coordination of oxygen by the alkali cation. Other than ice (see Chapter 15 by Hemley and Dera in this volume), the only simple oxide mineral of a monovalent cation, or hemi-oxide, is cuprite (Cu_2O).

The crystal structures of cuprite and its isomorph, Ag_2O , are cubic ($Pn3m$) with Cu or Ag at the $2a$ position with point symmetry $-43m$ and O in the $4b$ position with point symmetry $-3m$ as illustrated in Figure 1. This structure contains +1 cations in an unusual linear two-coordination, while each oxygen is coordinated to a tetrahedron of copper or silver cations. Both atom positions are fixed by symmetry, so that only the cubic cell parameter is required to define the structure. Bragg et al. (1965) point out that the structure consists of two interpenetrating systems of linked atoms that do not interconnect, indicating possible unusual behavior at elevated temperature or pressure.

Werner and Hochheimer (1982) studied cuprite and Ag_2O to pressures in excess of 24 GPa by X-ray powder diffraction. Cuprite transforms to a hexagonal structure at about 10 GPa and to the CdCl_2 structure above 18 GPa. Ag_2O transforms to the hexagonal structure at about 0.4 GPa and retains that structure to at least 29 GPa. The bulk modulus of the cubic cuprite structure is 131 GPa with $K' = 5.7$ (Table 1). At elevated temperature, cuprite breaks down to $\text{Cu} + \text{CuO}$ at about 450°C (Werner and Hochheimer 1982).

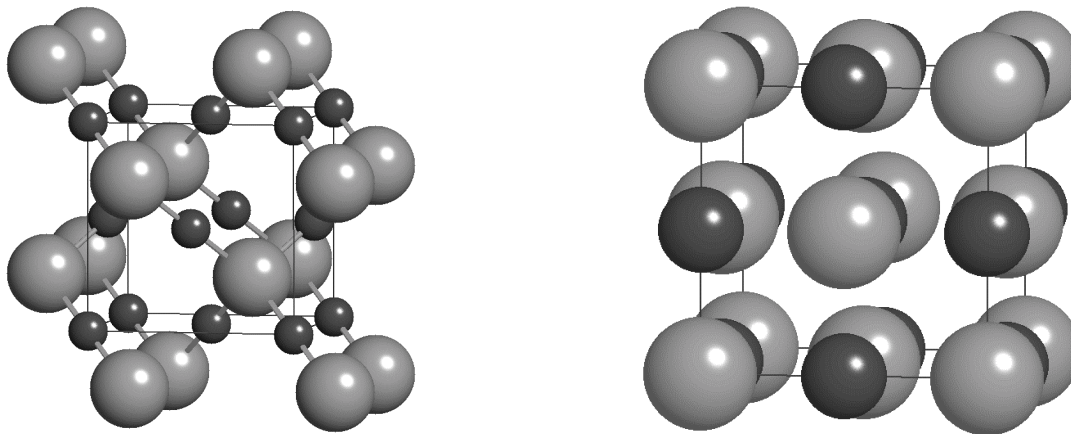


Figure 1. (left) The crystal structure of cuprite Cu_2O and Ag_2O . The structure is cubic ($Pn3m$) with the monovalent cation in linear two-fold coordination.

Figure 2. (right) The crystal structure of periclase (MgO). The structure is the same as that of halite (NaCl) or rocksalt and is cubic ($Fd3m$) with each anion and cation in regular six-coordination.

Table 1. Comparative crystal chemistry of single oxides.

<i>Structure</i> formula	phase	C_N^{cation}	Pmax (GPa)	compression		<i>Ref.</i>	expansion		<i>Ref.</i>
				K_{T0} (GPa)	$\partial K/\partial P$		T-range (K)	α_V (10^{-6} K^{-1})	
<i>cuprite</i>									
Cu ₂ O	cuprite		10	131	5.7	[1]			
<i>halite</i>									
MgO	periclase		23	160(2)	4.2*	[2]	77-1315	35.7	[3]
FeO	wüstite		5.5	153(2)	4*	[4]	293-873	33.9	[5]
CaO	lime		135	111(1)	4.2(2)	[6]	293-2400	33.5	[7]
NiO	bunsenite		30	199	4.1	[8]			
MnO	manganosite		8.1	148(1)	4*	[9]	293-1123	34.5	[10]
CdO	monteponite		8.1	148(1)	4*	[9]			
CoO			30	191	3.9	[8]			
BaO			10	66.2(8)	5.7*	[11]			
SrO			34	91(2)	4.4(3)	[12]			
EuO			13	97	4*	[13]			
<i>wurtzite</i>									
BeO	bromellite		5	212(3)	4*	[14]	298-1183	27(1)	[14]
		^{IV} Be		210	4*	[14]	298-1183	25(2)	[14]
<i>massicot</i>									
β -PbO	massicot		5	23(6)	18(2)	[15]			
<i>corundum</i>									
Al ₂ O ₃	corundum		8	257(6)	4*	[16]	293-2298	23.0	[17]
		^{VI} Al		276(30)	4*	[16]			
Fe ₂ O ₃	hematite		5.2	225(4)	4*	[18]	293-673	23.8	[5]
		^{VI} Fe		195(50)	4*	[18]			
Cr ₂ O ₃	eskolaite		5.7	238(4)	4*	[18]	293-1473	18.6	[5]
		^{VI} Cr		200(20)	4*	[18]			
V ₂ O ₃	karelianite		4.7	195(6)	4*	[18]	300-710	42.6	[19]
Ti ₂ O ₃			4.8	186(50)	4*	[19]	296-868	22.4	[20]
		^{VI} Ti					296-868	7.6	[20]
<i>rutile</i>									
TiO ₂	rutile		4.8	216(2)	7*	[21]	298-1883	29.1(1)	[22]
		^{VI} Ti		220(80)		[21]	298-1883	27.6	[22]
SiO ₂	stishovite		16	287(2)	6*	[23]	293-873	18.6(5)	[24]
		^{VI} Si		342		[23]			
SnO ₂	cassiterite		5.0	218(2)	7*	[21]			
		^{VI} Sn		180(80)		[21]			
GeO ₂	argutite		3.7	258(5)	7*	[21]			
		^{VI} Ge		270(80)		[21]			
RuO ₂			2.8	270(6)	4*	[21]			
		^{VI} Ru		220(120)		[21]			
<i>brookite</i>									
TiO ₂	brookite						293-898	24.6	[25]
<i>anatase</i>									
TiO ₂	anatase		4	190(10)	5(1)	[26]	293-1073	27.2	[27]
<i>baddeleyite</i>									
ZrO ₂	baddeleyite		10	95(8)	4*	[28]	293-1273	21.2	[5]
<i>fluorite</i>									
ThO ₂	thorianite			193(10)	4*	[29]	293-1273	28.5	[30]
UO ₂	uraninite		33	210(10)	7(2)	[31]	293-1273	24.5	[30]
HfO ₂			10	145	5*	[32]	293-1273	15.8	[5]

*Indicates fixed parameter.

References: [1] Werner and Hochheimer (1982)

[2] Fei (1999)

[3] Hazen (1976)

[4] Hazen (1981)

[5] Skinner (1966)

[6] Richet et al. (1988)

[7] Touloukian et al. (1977)

[8] Drickamer et al. (1966)

[9] Zhang (1999)

[10] Suzuki et al. (1979)

[11] Wier et al. (1986)

[12] Liu and Bassett (1973)

[13] Zimmer et al. (1984)

[14] Hazen and Finger (1986)

[15] Akaogi et al. (1992)

[16] Finger and Hazen (1978)

[17] Aldebert and Traverse (1984)

[18] Finger and Hazen (1980)

[19] McWhan and Remeika (1970)

[20] Rice and Robinson (1977)

[21] Hazen and Finger (1981)

[22] Sugiyama and Takéuchi (1991)

[23] Ross et al. (1990)

[24] Endo et al. (1986)

[25] Meagher and Lager (1979)

[26] Arlt et al. (2000)

[27] Horn et al. (1972)

[28] Leger et al. (1993a)

[29] Simmons and Wang (1971)

[30] Winslow (1971)

[31] Benjamin et al. (1981)

[32] Leger et al. (1993b)

Periclase group, AO

The monoxide group includes simple oxides of the divalent metals. At least 30 monoxide minerals and compounds are known, two-thirds of which crystallize in the cubic halite (B1) or rocksalt structure (space group $Fm\bar{3}m$; see figure 2) at room pressure and temperature. With the exception of the molecular solid carbon monoxide (CO; see Chapter 15 by Hemley and Dera in this volume), a structural classification of the naturally-occurring monoxides includes four major groups: rocksalt (MgO, FeO, CaO, NiO, and MnO); wurtzite (BeO and ZnO); litharge (PbO, SnO, PdO, and PtO); and tenorite (CuO and AgO), as reviewed by Liu and Bassett (1986).

The rocksalt structure monoxides, due to their structural simplicity, provide insight into the most fundamental concepts of crystal chemistry and phase transitions, such as the size, compressibility and thermal expansivity of cations and anions (Hazen and Prewitt 1977). Note, in particular, that the polyhedral bulk modulus and thermal expansion coefficient of the divalent cation octahedron in a periclase group oxide is identical to that of the bulk oxide. Recent compilations of thermal expansion (Fei 1995) and elasticity (Bass 1995) data are especially useful in this regard.

Bulk moduli and thermal expansion parameters for several natural and synthetic monoxides (the latter including BaO, SrO, and rare-earth monoxides) and their constituent polyhedra are listed in Table 1. Observed transition pressures (and temperatures) for various monoxides are given in Table 2, and radius-ratios, molar volumes, densities and compression parameters are recorded in Tables 3.

Periclase: Periclase (MgO) has been the subject of extensive studies at high-pressure and high-temperature. Periclase is also one of the few minerals for which no pressure-induced phase transition has been observed below 227 GPa (Duffy et al 1995), so that MgO composition will likely have the halite structure, even in Earth's the lower mantle. Pure MgO has become an internal standard material for experimental research at high pressure and temperature and, thanks to extensive testing, has widely accepted bulk properties. The isothermal bulk modulus of MgO is 160 ± 2 GPa with $K' = 4.15$ fixed from ultrasonics (Fei 1999), while the average thermal expansion coefficient to 1000°C is approximately $32 \times 10^{-6} \text{ K}^{-1}$ (Suzuki 1975).

Wüstite: Wüstite (Fe_{1-x}O) is a complex, non-stoichiometric (Fe-deficient) phase, which for a given composition may exhibit quite different physical properties (Hazen and Jeanloz 1984). This variability is due to structural differences resulting from short- and long-range ordering of defect clusters, as well as the presence of exsolution lamellae of magnetite Fe_3O_4 or metallic Fe on the scale tens of unit cells. The wüstite defect structure is expected to depend primarily on the ratio of octahedral to tetrahedral ferric iron, and on the degree of ordering of defect clusters resulting from tetrahedral Fe^{3+} . These features, in turn, depend on the synthesis conditions as well as the transitory conditions of the experiment. It is therefore necessary for any reports to specify synthesis conditions, including, for example, starting materials, oxygen fugacity, temperature, synthesis duration, and quench rate.

Stoichiometric FeO with the halite structure is not a stable phase below at least 10 GPa. At lower pressures, wüstite, (Fe_{1-x}O) is a complex, nonstoichiometric mineral with a nominal composition of $\text{Fe}_{1-3x}^{2+}\text{Fe}_{2x-x}^{3+}\text{O}^{2-}$, where x usually ranges from $0.04 < x < 0.12$. Ferric iron may occupy either the octahedral (VI) cation sites or the normally vacant tetrahedral (IV) interstitial sites. Therefore, if there are t tetrahedral Fe^{3+} , a more realistic structural formula becomes; $^{\text{VI}}[\text{Fe}_{1-3x}^{2+}\text{Fe}_{2x-t-x}^{3+}]^{\text{IV}}\text{Fe}_t^{3+}\text{O}^{2-}$.

Mao et al (1996) report that wüstite undergoes a phase transition to a rhombohedral hcp structure at 17 GPa and room temperature. At temperatures above 600 K, wüstite undergoes a first-order phase transition to the NiAs structure. Hazen (1981) measured the isothermal compressibility of single crystal wüstite with varying degrees of nonstoichiometry. The bulk modulus of wüstite is relatively independent of composition for $\text{Fe}_{0.91}\text{O}$, $\text{Fe}_{0.94}\text{O}$, and $\text{Fe}_{0.96}\text{O}$; Hazen (1981) reports bulk moduli of 152 ± 2 , 153 ± 2 , and 154 ± 2 GPa, respectively. The average thermal expansion coefficient to 1000°C is approximately $34 \times 10^{-6} \text{ K}^{-1}$ (Fei 1995).

Magnesiowüstite: Magnesiowüstite, (Mg,Fe)O of intermediate compositions, is the subject of relatively few studies, particularly on single crystals, due to the difficulty in synthesizing adequate samples. Reichmann et al. (2000) described the synthesis of high-quality single crystals of (Mg,Fe)O using the interdiffusion of Fe and Mg between magnesiowüstite powders and single-crystal periclase. Jacobsen et al. (1999) measured hydrostatic compression to 10 GPa on several of these (Mg,Fe)O single crystals, as summarized in Table 3. For more magnesium-rich compositions, magnesiowüstite bulk moduli appear to be approximately a linear function of $\text{Fe}/(\text{Fe}+\text{Mg})$. End member periclase and samples with $\text{Fe}/(\text{Fe}+\text{Mg}) = 0.27$ and 0.56 have bulk moduli of 160 ± 2 , 158 ± 1 , and 156 ± 1 , respectively. However, Jacobsen et al. (1999) report $K_{T0} = 151 \pm 1$ GPa for $\text{Fe}/(\text{Fe}+\text{Mg}) = 0.75$, while (Hazen 1981) reports $K_{T0} = 154 \pm 2$ for wüstite with maximal room-pressure Fe content.

Lime: Lime (CaO) has the halite (B1) structure at ambient P-T. A pressure-induced phase transition to the nickel arsenide (B2) structure was reported by Jeanloz et al. (1979) to occur at 60-70 GPa during both shock-wave and diamond-cell experiments. At room temperature, the transition was observed at 60 ± 2 GPa in the diamond-anvil cell, whereas in shock wave experiments, a transition thought to be the B1-B2, occurred between 63 and 70 GPa at approximately 1350 K. The transition is accompanied by an 11% decrease in volume. Several authors report the bulk modulus of CaO to be ~ 110 GPa (Bass 1995), while the average thermal expansion coefficient to 1000°C is $34 \times 10^{-6} \text{ K}^{-1}$ (Fei 1995).

Table 2. Distortions and structural phase transitions observed in dense monoxides at high pressure.

mineral	formula	structure	high-P struct observed	high-P structure and (transition pressure GPa)*	Reference
periclase	MgO	<i>halite</i>	No	< 227 GPa	Duffey et al. (1995)
wüstite	Fe _{1-x} O	<i>nominally halite</i>	Yes	rhomb hcp (17)	Mao et al. (1996)
lime	CaO	<i>halite</i>	Yes	NiAs (90 at 600K)	Richet et al. (1988)
bunsenite	NiO	<i>halite</i>	No	CsCl (60)	Drickamer et al. (1966)
manganosite	MnO	<i>halite</i>	Yes	< 30	Noguchi et al. (1996)
monteponite	CdO	<i>halite</i>	No	CsCl (90)	Drickamer et al. (1966)
zincite	ZnO	<i>wurtzite</i>	Yes	< 30	Jamieson (1970)
bromellite	BeO	<i>wurtzite</i>	No	NaCl (9)	Hazen and Finger (1986)
massicot	PbO	<i>litharge</i>	Yes	< 5.7	Adams et al. (1992)
				orth dist (0.7)	
				massicot (2.5)	
tenorite	CuO	<i>tenorite</i>	No	not investigated	
montroydite	HgO	<i>montroydite</i>	No	not investigated	
<i>Other monoxides</i>					
	CoO	<i>halite</i>	No	< 30	Drickamer et al. (1966)
	BaO	<i>halite</i>	Yes	NiAs (10) PH ₄ I (15)	Wier et al. (1986)
	SrO	<i>halite</i>	Yes	CsCl (36)	Sato and Jeanloz (1981)
	SnO	<i>litharge</i>	Yes	orth. dist (2.5)	Adams et al. (1992)
	EuO	<i>halite</i>	Yes	collapsed NaCl (30)	Jayaraman (1972)
				CsCl (40)	

*At room temperature unless otherwise specified.

Manganosite: The pressure-volume relationship of manganosite, MnO with the rocksalt structure, was first studied by Clendenen and Drickamer (1966), who used a Murnaghan equation of state to calculate $K_{T0}=144$ GPa with $K'=3.3$. A discontinuity was observed in their plot of a/a_0 versus pressure at approximately 10GPa, although they could say only that the high-pressure structure was tetragonal ($c/a=0.98$) or of lower symmetry. High-pressure behavior of MnO was investigated by static compression in a diamond-anvil press to 60 GPa by Jeanloz and Rudy (1987). Eulerian finite-strain EoS parameters for MnO were reported as $K_{T0}=162 \pm 17$ GPa with $K'=4.8 \pm 1.1$. No evidence for a structural transition was observed below 60 GPa. Shock compression experiments by Noguchi et al (1996), however, show that MnO does undergo the B1-B2 phase transition at about 90 GPa, resulting in a volume decrease of about 8%. They also point out that the pressure at which MnO undergoes this structural transition is consistent with a relationship between radius ratio $r_c:r_a$ and B1-B2 transition pressure observed for other alkaline earth monoxides, including CaO, SrO and BaO.

Zhang (1999) measured the volume compression of MnO and CdO simultaneously in the DAC to 8.1 GPa. The two phases have identical bulk moduli within experimental uncertainty, with $K_{T0} = 148 \pm 1$ GPa fixing $K' = 4$. The average thermal expansion coefficient to 1000°C is $35 \times 10^{-6} \text{ K}^{-1}$ (Suzuki et al 1979).

General Crystal Chemical Trends: The structures of periclase-type oxides display striking systematic trends as functions of temperature and pressure. For example, the volume thermal expansion coefficient, α_v , of all reported oxides, including NiO, MgO, CdO, FeO, MnO and CaO, are within $\pm 6\%$ of an average value $\alpha_v = 34 \times 10^{-6} \text{ K}^{-1}$ (see Table 1), in spite of more than 50% variation in molar volume between NiO and CaO. These data are reflected in the formulation of Hazen and Prewitt (1977), as modified by Hazen and Finger (1982), that the volume thermal expansion coefficient of cation-oxygen polyhedra, α_p , is to a first approximation dependent on cation valence divided by coordination number, z/n , but is independent of bond length. Thus, they proposed the empirical relationship:

$$\alpha_p \sim 12 \times 10^{-6} \cdot (n/z) \text{ K}^{-1} \quad (\text{equation 1})$$

We will examine this relationship, in particular noting its limitations in application to cations of valence $>+2$, in subsequent discussions of high-temperature oxide structures.

Bulk moduli of periclase-type oxides, in contrast to thermal expansivities, vary significantly with unit-cell (or molar) volume (Table 3). To a first approximation, these oxides conform to the well-known bulk modulus-volume (K-V) relationship (Anderson and Nafe 1965, Anderson and Anderson 1970), which was originally applied to molar volumes of isostructural compounds:

$$K \times V = \text{constant.}$$

In this formulation, a different constant applies to each isoelectronic structure type. Thus, for example, in the periclase-type oxides:

for MgO: $K = 160$ GPa	$V = 74.7 \text{ \AA}^3$	$K \times V = 11952 \text{ GPa} \cdot \text{\AA}^3$
for CaO: $K = 111$ GPa	$V = 111.3 \text{ \AA}^3$	$K \times V = 12354 \text{ GPa} \cdot \text{\AA}^3$
for BaO: $K = 66.2$ GPa	$V = 167.0 \text{ \AA}^3$	$K \times V = 11058 \text{ GPa} \cdot \text{\AA}^3$

Hazen and Finger (1979a, 1982) extended this empirical relationship by considering the product of polyhedral bulk modulus (K_p) and cation-oxygen bond distance cubed (d^3), which is a fictive volume term, as described in Chapter 5 by Hazen and Prewitt in this volume. They proposed that:

$$(K_p \times d^3)/z = \text{constant},$$

where z is the cation formal valence. In the special case of periclase, $K = K_p$, while $d^3 = (1/8)V$ and $z = 2$. Thus, because of this simple scaling, the $K_p \times d^3$ relationship holds for cation octahedra in periclase-type structures:

$$(K_p \times d^3)/z \sim 750 \text{ GPa-}\text{\AA}^3 \quad (\text{equation 2})$$

Thus,

$$K_p \sim 750 (z/d^3) \text{ GPa} \quad (\text{equation 3})$$

Applying equation 3 to periclase-type oxides, predicted octahedral bulk moduli for MgO, CaO and BaO are 161, 108, and 72 GPa, compared to observed values of 160, 111, and 66 GPa, respectively.

This polyhedral bulk modulus-volume relationship differed from that of previous authors in that it can be applied to direct comparisons of cation polyhedral behavior for similar polyhedra in disparate structure types. We will consider this empirical relationship, in particular its limitations when applied to polyhedra of relatively high charge density (i.e., coordination number <6 or formal cation valence $>+2$), in subsequent sections.

Zincite group, AO

Zincite (ZnO) and bromellite (BeO) crystallize in the hexagonal wurtzite structure (space group $P6_3mc$) at ambient conditions. In this structure, illustrated in figure 3, every atom is in tetrahedral coordination, so that each cation is bonded to four oxygens and each oxygen is bonded to four cations. The structure has the divalent cation fixed by symmetry at $(1/3, 2/3, 0)$ and oxygen at $(1/3, 2/3, z)$; thus, z (~ 0.375) is the only structural parameter other than unit-cell axes a and c .

Bromellite: Hazen and Finger (1986) refined the structure of bromellite at six pressures to 5 GPa and at five temperatures to 1180 K. The axial ratio c/a does not change with pressure to 5 GPa, so the axial compression of BeO is isotropic. The bulk modulus of BeO was calculated to be 212 ± 3 GPa assuming $K' = 4$. The z parameter of oxygen also does not change significantly with pressure, and increases only very slightly with temperature, so the structure simply scales with the changing molar volume. The BeO_4 polyhedral modulus is 210 GPa, while the Be-O mean distance in bromellite is ~ 1.65 \AA. The predicted tetrahedral bulk modulus is 334 GPa – a value significantly greater than that observed for octahedra in periclase-type oxides.

The high-temperature structure of bromellite was determined by Hazen and Finger (1986), who reported a BeO_4 tetrahedral thermal expansion coefficient of $25 \times 10^{-6} \text{ K}^{-1}$. This value matches the $24 \times 10^{-6} \text{ K}^{-1}$ estimate of the Hazen and Finger (1982) empirical relationship (equation 1).

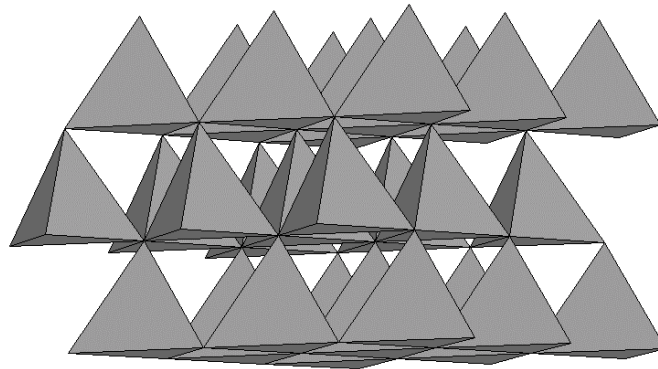


Figure 3. (left) The crystal structure of bromellite (BeO). The structure is the same as that of wurtzite (ZnS) and is hexagonal ($P6_3mc$) with each cation and anion in regular four-coordination.

Table 3. Compression of rock-salt structure monoxides.

mineral	formula	rc:ra*	mol. volume (cm ³ /mol)	ρ calc (g/cm ³)	$\partial K/\partial P$	K _{T0} (GPa)	Pmax (GPa)	Reference
periclase	MgO	0.51	11.26	3.58	4.2*	160(2)	23	Fei (1999)
ferropericlase	(Mg _{0.73} Fe _{0.26} 0.01)O [†]	–	11.54	4.23 [†]	5.5(2)	158.4(7)	7	Jacobsen et al. (1999)
magnesiowüstite	(Mg _{0.42} Fe _{0.54} 0.04)O [†]	–	11.98	4.84 [†]	5.5(2)	156(1)	9	Jacobsen et al. (1999)
magnesiowüstite	(Mg _{0.24} Fe _{0.72} 0.04)O [†]	–	12.18	5.25 [†]	5.6(3)	151.3(7)	10	Jacobsen et al. (1999)
wüstite	Fe _{0.94} O	0.56	12.24	5.87 ^{††}	4*	153(2)	5.5	Hazen (1981)
lime	CaO	0.71	16.76	3.35	4.2(2)	111(1)	135	Richet et al. (1988)
bunsenite	NiO	0.49	10.91	6.85	4.1	199	30	Drickamer et al. (1966)
manganosite	MnO	0.48	13.22	5.37	4*	148(1)	8.1	Zhang (1999)
montepionite	CdO	0.68	15.52	8.27	4*	148(1)	8.1	Zhang (1999)
	CoO	0.53	11.62	6.45	3.9	191	30	Drickamer et al. (1966)
	BaO	0.97	25.18	6.09	5.7*	66.2(8)	10	Wier et al. (1986)
	SrO	0.81	22.05	4.70	4.4(3)	91(2)	34	Liu and Bassett (1973)
	EuO	0.84	20.36	8.25	4*	97	5	Zimmer et al. (1984)

*Shannon and Prewitt (1969) or revised values of Shannon and Prewitt (1970)

[†]Calculated densities for (Mg,Fe)O are corrected for non-stoichiometry; Fe³⁺ determined by mössbauer spectroscopy.

^{††}Ideal density.

Zincite: Jamieson (1970) observed a phase transition in ZnO from the wurtzite to rocksalt structure at 9 GPa and room temperature. The phase transition increases the coordination of both Zn and O from four to six. The transition was found to be reversible; however, reversal was successful only in the presence of NH₄Cl. Liu (1977) decomposed Zn₂GeO₄ and Zn₂SiO₄ at greater than 20 GPa and 1000°C and found the complete conversion to oxide components with Zn₂GeO₄ completely converting to the ZnO(II)-rocksalt phase, whereas Zn₂SiO₄ was found to break down into a mixture of ZnO(II) and wurtzite. This observation demonstrated that NH₄Cl was not necessary as a catalyst for the formation of ZnO in the rocksalt structure. Liu (1977) used the positions of six diffraction peaks to determine the cell parameter of the ZnO(II) rocksalt structure as $a = 4.275 \pm 2$ Å, which implies a zero-pressure volume change for the ZnO(I)-ZnO(II) phase transition of about 18 percent.

Other Monoxides

Litharge is the red, low-temperature polymorph of PbO (tetragonal, space group *P4/nmm*), whereas massicot is the yellow, high-temperature polymorph (orthorhombic, space group *Pbcm*). Surprisingly, the high-temperature massicot form is about 3.3% more dense than litharge, but both phases possess relatively open, low-density structures. Romarchite, (α -SnO) is isostructural with litharge. Adams et al (1992), who measured the compression of litharge, massicot and romarchite, report a bulk modulus of 22.7 ± 6 GPa for massicot, but do not report bulk moduli or their original cell data for litharge or romarchite. They observe an orthorhombic distortion of the tetragonal litharge and romarchite structures at 1.0 and 2.5 GPa, respectively. Atom position data were not reported for any of these structures, nor does it appear that either tenorite (CuO) or montroydite (HgO) structures have yet been studied at elevated temperature or pressure.

Corundum group, A₂O₃

The high-pressure crystal chemistry of corundum, α -Al₂O₃, is of particular interest to mineral physics, owing to the common use of the ruby fluorescence scale as a means of pressure measurement in diamond-anvil experiments. In addition, there is the significant possibility that the corundum-type structure would host aluminum or chrome in the Earth's mantle. No high-pressure or high-temperature phase transitions have been observed in corundum.

At ambient conditions, the corundum structure, illustrated in Figure 4, is trigonal ($R\bar{3}c$). This structure is common to corundum (Al₂O₃), hematite (Fe₂O₃), eskolaite (Cr₂O₃), and karelianite (V₂O₃), as well as to Ti₂O₃ and Ga₂O₃. The one symmetrically-distinct oxygen atom in the corundum-type structure is coordinated to four trivalent cations. Oxygen atoms form a nearly ideal hexagonal close-packed array. The cation layers formed by the packing direction are 2/3 occupied by the six-coordinated trivalent cation, such that each sheet is dioctahedral, or gibbsite-like in nature. Six of these layers repeat in the *c* direction. In the *R*-centered setting, the trivalent cation occupies the octahedral site at (0, 0, *z*) and the oxygen is placed at (*x*, 0, 1/4). In the ideal hexagonal close-packed structure, z_{Al} and x_O would be 1/3 and the *c/a* ratio would be 2.833.

The high-pressure and high-temperature structural behavior of various sesquioxides are summarized in Tables 1, 4, 5, and 6.

Corundum: Finger and Hazen (1978) refined the crystal structure of ruby (with 0.4 mol% Cr³⁺) at six pressures to 4.6 GPa and found that the *z* parameter of Al and the *x* parameter of oxygen remain constant within experimental error, with $z_{Al}=0.3521 \pm 2$ and $x_O=0.3065 \pm 8$. The measured linear compression of the axial directions are only slightly anisotropic with $\beta_a = 1.36$ and $\beta_c = 1.22$ (both $\times 10^{-3}$ GPa⁻¹), so the *c/a* ratio remains essentially constant at 2.73 up to 4.6 GPa. Compression of the corundum structure is thus very uniform, and does not approach the ideal HCP structure.

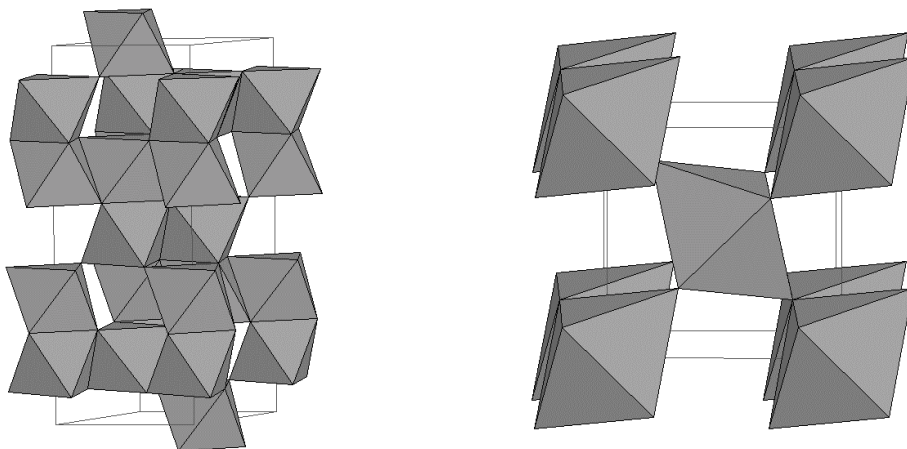


Figure 4. (left) The crystal structure of corundum ($\alpha\text{-Al}_2\text{O}_3$). The structure is trigonal ($R\bar{3}c$) (c -vertical) with all cations equivalent and in six-coordination. The structure has two out of three octahedral sites in each layer occupied and each octahedron shares one face with octahedra in the adjacent layer.

Figure 5. (right) The crystal structure of rutile (TiO_2), c -axis projection. The structure is tetragonal ($P4_2/mnm$), with each tetravalent cation in six-coordination. The octahedra form edge-sharing chains parallel to c .

Compressibility and thermal expansion of Al_2O_3 -type compounds are summarized in Table 1, while various high-temperature and high-pressure studies of corundum are summarized in Tables 4 and 5, respectively.

Eskolaite: Similar compression behavior was found for eskolaite (Cr_2O_3) by Finger and Hazen (1980), who refined the structure at four pressures to 5.7 GPa. As with $\alpha\text{-Al}_2\text{O}_3$, the linear axial compressibility is quite isotropic, as the c/a ratio remains essentially constant at 2.74 within error, and the atom position parameters z_{Cr} and x_{O} remain statistically constant over the experimental pressure range with $z_{\text{Cr}}=0.35$ and $x_{\text{O}}=0.31$.

Both Al_2O_3 and Cr_2O_3 are known to exhibit nonstoichiometric spinel modifications, whereby the normally six-coordinate cation occupies both octahedral and tetrahedral sites. This structural change decreases the overall packing efficiency of the structure from the ideal corundum packing in Cr_2O_3 , for example, by about 13% (Liu and Bassett 1986). A possible first-order phase transition was observed in Cr_2O_3 at 14 GPa during resistivity measurements (Minomura and Drickamer 1963), although the structure was not investigated.

Hematite: Hematite, $\alpha\text{-Fe}_2\text{O}_3$, is nominally a corundum-type structure although at ambient conditions the nonstoichiometric spinel and C-type structures have also been observed. High-pressure structure determinations of $\alpha\text{-Fe}_2\text{O}_3$ were made up to 5.2 GPa by Finger and Hazen (1980). In contrast to ruby, the linear axial compression of hematite is rather anisotropic with c approximately 25% more compressible than the a -direction. However, for all three of the structures $\alpha\text{-Al}_2\text{O}_3$, Cr_2O_3 , and $\alpha\text{-Fe}_2\text{O}_3$ in the rhombohedral setting, the interaxial angle, α , remains constant while only the a -dimension shortens linearly. The atom position parameters of hematite, as in $\alpha\text{-Al}_2\text{O}_3$ and Cr_2O_3 , remain constant over the pressure range studied and so also should not be expected to approach the ideal HCP lattice.

V_2O_3 : Compression of V_2O_3 is significantly greater than that of $\alpha\text{-Al}_2\text{O}_3$, Cr_2O_3 , and $\alpha\text{-Fe}_2\text{O}_3$ (Finger and Hazen 1980), recorded in Tables 1, 5 and 6. The lattice compression of V_2O_3 is strongly anisotropic and marked by an increase in the c/a ratio from 2.83 at room pressure to 2.85 at 4.7 GPa. The atom position parameters of V_2O_3 approach the ideal HCP structure, becoming close to z_{V} and $x_{\text{O}} = 1/3$, while the c/a ratio remains close to 2.83. The linear axial compressibility in the a direction is about 3 times that of the c direction. Similarly, McWhan and Remeika (1970) observed anisotropic compression for Ti_2O_3 .

At high temperature, the V_2O_3 structure is observed to move away from the ideal HCP structure (Robinson 1975). The atom position parameters, z_{V} and x_{O} , both diverge from $1/3$ while the c/a ratio decreases from the nearly ideal value of 2.38 at room temperature. It is fundamental to note that this response is the inverse of the high pressure changes in V_2O_3 towards the HCP structure, revealing the inverse character of the structural responses to high pressure and high temperature that has been observed for many simple compounds.

General Crystal Chemical Trends: Equation 1 predicts that trivalent cation-oxygen octahedra will have $\alpha_{\text{p}} \sim 12 \times 10^{-6} \times (n/z) \text{ K}^{-1} = 24 \times 10^{-6} \text{ K}^{-1}$. This prediction matches the observed values of 23.0, 23.8, and $22.4 \times 10^{-6} \text{ K}^{-1}$ for Al_2O_3 , Fe_2O_3 , and Ti_2O_3 , respectively (Tables 1 and 4). However, the observed thermal expansivity of Cr_2O_3 of $18.6 \times 10^{-6} \text{ K}^{-1}$ is significantly less than the predicted value. The reasons for this difference are not obvious, and further high-temperature structural investigation of the transition metal sesquioxides is thus warranted.

Using a first-order Birch-Murnaghan equation of state with $K' = 4$, the observed bulk moduli for the X_2O_3 compounds $\alpha\text{-Al}_2O_3$, Cr_2O_3 , $\alpha\text{-Fe}_2O_3$ and V_2O_3 are 257 ± 6 , 238 ± 4 , 225 ± 4 and 195 ± 6 GPa, respectively. Of these compounds, oxides of Al, Cr, and Fe closely conform to a bulk modulus-volume relationship. The bulk modulus of V_2O_3 , however, is anomalously low, for reasons that are not obvious.

The octahedral bulk moduli of corundum-type structures are nearly identical to the bulk modulus of the oxides (Table 6). Applying equation 3, predicted polyhedral bulk moduli for Al, Cr, Fe and V sesquioxides are 321, 286, 269 and 276 GPa, respectively. Predicted values of Al, Cr and Fe oxides are 20 to 25% larger than observed values, while that of V_2O_3 is 40% larger than observed. The predicted and observed relative values of $\alpha\text{-Fe}_2O_3$ and V_2O_3 polyhedral moduli, furthermore, are reversed.

Table 4. Linear thermal expansion coefficients for corundum-type sesquioxides.

mineral name	corundum	eskolaite	hematite
Formula	$\alpha\text{-Al}_2O_3$	Cr_2O_3	$\alpha\text{-Fe}_2O_3$
T range	296-2298 K	296-1473 K	296-673 K
Expansion coefficients	$(10^{-6} K^{-1})$		
α_v	23.0	18.6	23.8
α_a	7.3		7.9
α_c	8.3		8.0
Reference	Aldebert & Traverse (1984)	Skinner (1966)	Skinner (1966)

Table 5. Compression of Al_2O_3 at 300K.

mineral name	corundum	ruby	ruby	ruby
Formula	$\alpha\text{-Al}_2O_3$	$\alpha\text{-Al}_2O_3$ (0.4mol% Cr^{3+})	$\alpha\text{-Al}_2O_3$ (0.05mol% Cr^{3+})	$\alpha\text{-Al}_2O_3$ (0.05mol% Cr^{3+})
Sample	synthetic	synthetic	synthetic	synthetic
Pmax (Gpa)	12.1	4.6	9	50
K_{T0} (GPa)	239(4)	257(6)	254(2)	253(1)
K'	0.9(8)	4*	4.3(1)	5.0(4)
Axial compression				
β_a ($10^{-3} GPa^{-1}$)	1.34	1.22(3)		
β_c	1.37	1.36(3)		
Site bulk moduli (GPa)				
M-site		276(30)		
Reference	Sato&Akimoto (1979)	Finger&Hazen (1978)	d'Amour et al. (1978)	Richet et al. (1988)

* Indicates fixed parameter

Table 6. Compression of Cr_2O_3 , V_2O_3 , and $\alpha\text{-Fe}_2O_3$ at 300 K.

mineral name	eskolaite	eskolaite	karelianite	karelianite	hematite	hematite
Formula	Cr_2O_3	Cr_2O_3	V_2O_3	V_2O_3	$\alpha\text{-Fe}_2O_3$	$\alpha\text{-Fe}_2O_3$
Sample	synthetic	synthetic	synthetic	synthetic	synthetic	synthetic
Pmax (Gpa)	5.7	11.3	4.7	11.1	5.2	11.1
K_{T0} (GPa)	238(4)	231(5)	195(6)	175(3)	225(4)	231 (< 3 GPa)
K'	4*	2(1)	4*	3.1(7)	4*	4*
Axial compression						
β_a ($10^{-3} GPa^{-1}$)	1.36	1.33	2.16	2.12	1.23	1.31
β_c	1.25	0.90	0.51	0.99	1.76	2.01
Site bulk moduli (GPa)						
M-site	200(20)				195(50)	
Reference	Finger&Hazen (1980)	Sato&Akimoto (1979)	Finger&Hazen (1980)	Sato&Akimoto (1979)	Finger&Hazen (1980)	Sato&Akimoto (1979)

*Indicates fixed parameter.

Rutile Group, AO_2

Rutile (TiO_2) and its isomorphs, which display a tetragonal (space group $P4_2/mnm$) structure, represent the most common structure-type of naturally occurring XO_2 dioxides. Rutile is the ambient structure type of cassiterite (SnO_2), pyrolusite (MnO_2), and plattnerite (PbO_2), as well as GeO_2 , RuO_2 , and several other synthetic compounds. In addition, one of the naturally occurring, high-pressure polymorphs of SiO_2 , stishovite, crystallizes with the rutile structure. Thus, the high-pressure behavior of rutile-type dioxides is of considerable importance to mantle mineralogy.

The rutile structure, illustrated in Figure 5, features edge-sharing XO_6 octahedral strips that run parallel to the c -axis. Each strip is linked to four others by corner-sharing oxygen. This arrangement of octahedral strips causes the structural compression and thermal expansion to be highly anisotropic. The structure has only two symmetrically distinct atoms; the X cation at the origin (0,0,0) and the oxygen at ($x,x,0$) with $x \sim 0.3$, so there is only one variable atomic position parameter in the structure. This parameter, plus the tetragonal cell dimensions a and c , are thus all that are required to define the structure.

Hazen and Finger (1981) investigated the high-pressure crystal structures of rutile-type dioxides, TiO_2 , SnO_2 , GeO_2 , and RuO_2 , while Kudoh and Takeda (1986) measured the high-pressure structure of TiO_2 . In all four compounds the a -direction is approximately twice as compressible as c , so the c/a ratio increases with increasing pressure. Bulk moduli TiO_2 , SnO_2 , and GeO_2 , are 216 ± 2 , 218 ± 2 , and 258 ± 5 GPa, respectively, assuming $K' = 7$ [as reported by Manghnani (1969) and Fritz (1974)]. The bulk modulus of RuO_2 is 270 ± 6 , assuming $K' = 4$ (Hazen and Finger 1981), while that for rutile-type SiO_2 is 313 ± 4 with $K' = 1.7 \pm 0.6$ (Ross et al. 1990).

Rutile: Rutile displays unusual high-pressure, high-temperature behavior, in that it dramatically violates the “inverse relationship” of pressure and temperature. Many ionic structures tend to vary in such a way that structural changes with increasing pressure mirror those with increasing temperature. In other words, raising the pressure has the same structural effect as lowering the temperature - both of which decrease the molar volume (figure 6a). High-temperature structure refinements of rutile between 25-400°C (Endo et al. 1986), 25-900°C (Meagher and Lager 1979), and 25-1600°C (Sugiyama and Takéuchi 1991) confirm that the oxygen parameter x does not change significantly below at least 1000°C. Similarly, the x parameter of oxygen does not change significantly with pressure below 5 GPa (Hazen and Finger 1981, Kudoh and Takeda 1986). However, the c and a axial directions of rutile compress and thermally expand anisotropically such that c/a increases both with increasing temperature and with increasing pressure (figure 6b). Therefore, the inverse relationship of pressure and temperature does not appear to hold for rutile, suggesting that the structure is not as strongly controlled by molar volume as most ionic structures. Bonding in rutile may thus be considerably more covalent than predicted by the crystal structure alone (Hazen and Finger 1981).

Figure 6. The inverse relationship between structural changes with temperature and pressure. (a) The ideal case occurs when structural parameters are a function of molar volume, as expressed by V/V_o . (b) The c/a of rutile (TiO_2) increases both with increasing pressure and with increasing temperature. High-pressure data are from Hazen and Finger (1981), high-temperature data are from Meagher and Lager (1979), and low-temperature data are from Samara and Peercy (1973).

Stishovite: Stishovite, the rutile-type high-pressure polymorph of SiO₂ is stable at pressures greater than 10 GPa. The density of stishovite is about 4.3 g/cm³, which is about 46% more dense than coesite. The crystal structure of stishovite was investigated at pressures to 6 GPa by Sugiyama et al. (1987) and to 16 GPa by Ross et al. (1990). The axial compressibility of stishovite is similar to rutile, with the *a*-axis approximately twice as compressible as *c*, so the *c/a* ratio also increases with increasing pressure. Axial compressibilities determined by Ross et al. (1990) are $\beta_a = 1.19 \cdot 10^{-3} \text{ GPa}^{-1}$ and $\beta_c = 0.13 \cdot 10^{-3} \text{ GPa}^{-1}$.

The large axial compression anisotropy of rutile-type compounds can be attributed to the strong metal cation-cation (and oxygen-oxygen) repulsion across (and along) the edge sharing chain of octahedra. Ross et al. (1990) report for the isothermal bulk modulus of stishovite $K_{T0} = 313 \pm 4 \text{ GPa}$, with $K' = 1.7 \pm 6$. If, however, K' is assumed to be 6, closer to other rutile-type structures, a value of $K_{T0} = 287 \pm 2 \text{ GPa}$ is obtained. The SiO₆ octahedron compresses linearly below 16 GPa, with a polyhedral bulk modulus of 342 GPa.

Unlike rutile, stishovite appears to follow the inverse law of pressure and temperature. Ito et al. (1974) report stishovite thermal expansion and Endo et al. (1986) investigated the crystal structure of stishovite at several temperatures to 400°C. These authors report linear thermal expansion coefficients for the axial direction $\alpha_a = 7.5 \pm 2 \cdot 10^{-6} \text{ K}^{-1}$ and $\alpha_b = 3.8 \pm 3 \cdot 10^{-6} \text{ K}^{-1}$. So, for stishovite, the ratio *c/a* increases with increasing pressure and decreases with increasing temperature. This is the expected result for most ionic structures in that the effects of pressure and temperature on the molar volume are rutile-type compounds are summarized in Tables 7, 8 and 9.

General Crystal Chemical Trends of Rutile-Type Oxides: Octahedral bulk moduli for the *X* = Sn, Ru, Ti, Ge, and Si *X*⁴⁺O₆ groups are calculated from the high-pressure structure refinements as 180, 220, 220, 270, and 340 GPa, respectively, in order of increasing bulk modulus. Mean cation-oxygen bond distances for these five compositions decrease in the same order: 2.054, 1.970, 1.959, 1.882, and 1.775 Å, respectively. Thus, a bulk modulus-volume relationship holds for rutile-type oxides, as well as for their constituent cation octahedra. However, predicted octahedral bulk moduli for these five dioxides, calculated from equation 3, are 346, 392, 399, 450, and 536 GPa, which are significantly greater than observed moduli.

Similarly, the observed polyhedral thermal expansion coefficient of TiO₆ octahedra in rutile (Meagher and Lager 1979, Sugiyama and Takeuchi 1991) is approximately $26 \times 10^{-6} \text{ K}^{-1}$, which is more than twice the $12 \times 10^{-6} \text{ K}^{-1}$ value predicted by equation 1. These results point to the severe limitations of the empirical equations 1 and 3 in dealing with nominally tetravalent cations.

Brookite and Anatase

In addition to rutile, titanium dioxide exists in several polymorphs, including orthorhombic brookite (space group *Pbca*; figure 7) and tetragonal anatase (space group *I4₁/amd*; figure 8) at low pressure. These structures both feature Ti in six coordination, but they differ in the arrangement of TiO₆ octahedra and the number of their shared edges (Maeger and Lager 1979). Rutile, brookite, and anatase have two, three, and four shared edges per octahedron, respectively. In all three structures the octahedral arrangement is relatively inflexible; Ti-O-Ti angles cannot vary without distortions to individual octahedra. Bulk moduli and volumetric thermal expansion (Tables 1, 7, and 8), therefore, reflect primarily the behavior of the constituent TiO₆ octahedra.

High-pressure structure studies are not yet available for brookite or anatase. Horn et al. (1972) reported high-temperature structure refinements for anatase to 800°C, and Meagher and Lager (1979) documented structures of brookite to 625°C and rutile to 900°C. Rutile and anatase both displayed linear increases in octahedral volume with increasing temperatures, with similar average volumetric thermal expansion coefficients of 25 and $26 \times 10^{-6} \text{ K}^{-1}$, respectively. The TiO₆ octahedra in brookite, on the other hand, showed no significant polyhedral expansion between room temperature and 300°C, but an average volumetric expansion of about $30 \times 10^{-6} \text{ K}^{-1}$ above that temperature. Meagher and Lager (1979) suggested that the unusual behavior of brookite results from the off-centered position of the octahedral Ti cation. Increased thermal vibration amplitude causes this cation to approach the centric position at high temperature.

Other Dioxide Structures

Baddeleyite (ZrO₂, monoclinic space group *P2₁/c*), is the ambient structure of zirconia, as well as a high-pressure form of TiO₂ (Simons and Dacheille 1967, Arlt et al. in press). This structure, illustrated in figure 10, transforms reversibly to an orthorhombic variant (space group *Pbcm*) at approximately 3.5 GPa (Arashi and Ishigame 1982). This transformation was investigated with high-pressure, single-crystal x-ray diffraction by Kudoh et al (1986), who reported the ZrO₂ structure at four pressures to 5.1 GPa. Over this pressure range Kudoh et al. found the Zr-O bonds to be relatively incompressible, with average Zr-O distances of $2.16 \pm 1 \text{ \AA}$ at room pressure and $2.14 \pm 3 \text{ \AA}$ at 5.1 GPa. These results suggest a ZrO₆ polyhedral bulk modulus in excess of 200 GPa. This value is significantly greater than the observed $95 \pm 8 \text{ GPa}$ ($K'=4$) bulk modulus of monoclinic baddeleyite (Leger et al. 1993a), because low-pressure baddeleyite can accommodate volume changes through changes in Zr-O-Zr angles. However, Kudoh et al. (1986) find the bulk modulus of the less-tilted orthorhombic form to be approximately 250 GPa, similar to that of the constituent polyhedra.

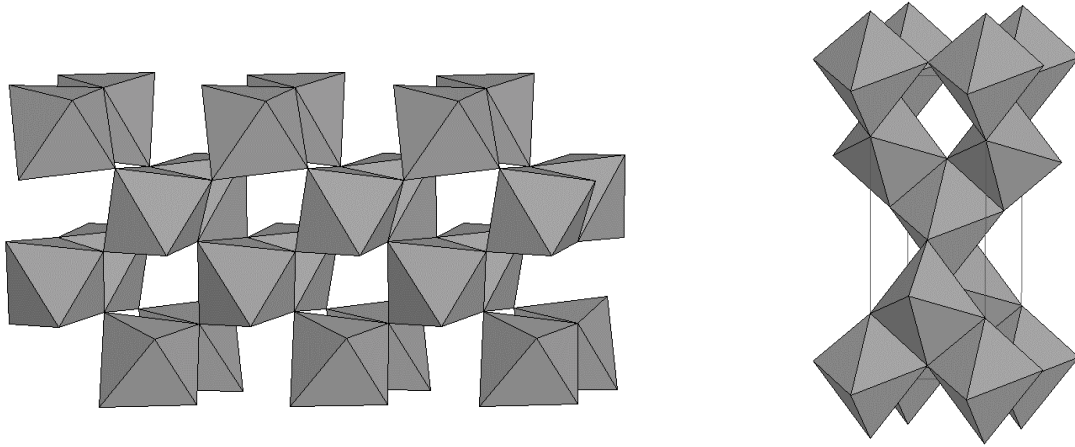


Figure 7. (left) The crystal structure of brookite (TiO_2), c -axis projection. The structure is orthorhombic ($Pbca$) with each tetravalent cation in six-coordination.

Figure 8. (right) The crystal structure of anatase (TiO_2), c -axis projection. The structure is tetragonal ($I4_1/amd$) with each tetravalent cation in six-coordination.

Additional pressure-induced phase transitions in ZrO_2 and HfO_2 have been investigated by Leger et al. (1993a, b) at room temperature to 50 GPa. Four successive first-order phase transitions were observed. Baddeleyite in its monoclinic and orthorhombic variants is stable up to about 10 GPa. An orthorhombic-I phase (space group $Pbca$) is stable between 10 and 25 GPa, an orthorhombic-II phase occurs between 25 and 42 GPa, and an orthorhombic-III phase was found to be stable above 42 GPa, though the authors were unable to determine the space group of the orthorhombic II and III phases.

Three dioxide minerals, cerianite (CeO_2), uraninite (UO_2), and thorianite (ThO_2), have the cubic fluorite structure (space group $Fm\bar{3}m$) with no variable atomic position parameters, so that the structure is fully determined by the unit cell parameter alone (see figure 11). The structure has the tetravalent cations in cubic eight-fold coordination, so there is no non-polyhedral volume in the structure and the bulk modulus of the structure is identical to that of the coordination polyhedra. Hazen and Finger (1979b) studied compression of uraninite to 5 GPa using single crystal methods and reported a bulk modulus of 230 ± 8 GPa and $K' = 3.7 \pm 3.6$. Benjamin et al (1981) studied the compression of uraninite to 650 GPa using powder diffraction methods and observed a transition to an orthorhombic structure, thought to be the PbCl_2 structure, at about 350 GPa. They report that the cubic structure has an isothermal bulk modulus of 210 ± 10 GPa with a K' of 7 ± 2 . Given the observed U-O distance ~ 2.37 Å and $z = 4$, the predicted polyhedral bulk modulus from equation 3 is 225 GPa, a value close to the observed modulus.

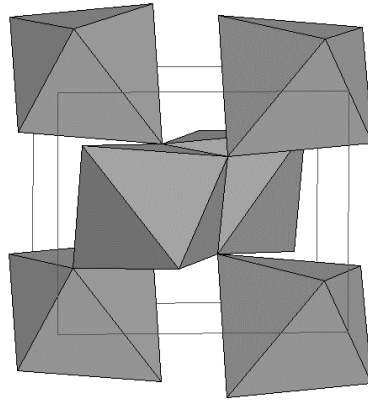


Figure 9. The crystal structure of $\alpha\text{-PbO}_2$. The structure is orthorhombic ($Pbcn$) with each cation in octahedral coordination.

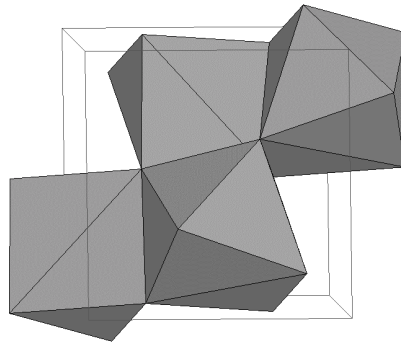


Figure 10. The crystal structure of baddeleyite (ZrO_2). The structure is monoclinic ($P2_1/c$) with each Zr in irregular seven-fold coordination.

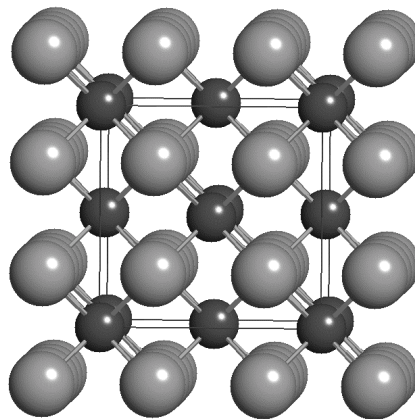


Figure 11. The crystal structure of uraninite (UO_2). This is the fluorite structure and is cubic ($Fm3m$) with each cation in cubic eight-fold coordination.

Table 7. Compression of rutile-type structures.

mineral name	stishovite	stishovite	cassiterite		
Formula	SiO ₂	SiO ₂	SnO ₂	GeO ₂	RuO ₂
Sample	synthetic	synthetic	synthetic	synthetic	synthetic
P _{max} (GPa)	16 GPa	6.1 GPa	5.0	3.7	2.8
K _{T0} (GPa)	313(4) [287(2)]	313(4)	224(2) [218(2)]	265(5) [258(5)]	270(6)
K'	1.7(6) [6]	6*	4* [7]	4* [7]	4*
Axial compression					
β _a (10 ³ GPa ⁻¹)	1.19	1.22	1.73	1.52	1.5
β _c	0.68	0.64	0.78	0.59	0.6
Site bulk moduli (GPa)					
M-site	342	250	180	270	220
Reference	Ross et al. (1990)	Sugiyama et al. (1987)	Hazen and Finger (1981)	Hazen and Finger (1981)	Hazen and Finger (1981)

* Indicates fixed parameter

Values in brackets give alternative fitting

Table 8. Compression of the TiO₂ polymorphs.

mineral name	rutile	anatase	α-PbO ₂ type	baddeleyite type
Formula	TiO ₂	TiO ₂	TiO ₂	TiO ₂
Sample	synthetic	synthetic	synthetic	synthetic
P _{max} (GPa)	4.8	4		10
K _{T0} (GPa)	222(2) [216(2)]	179(2)	290(15)	258(10)
K'	4* [7]	4.5(1.0)	4*	4.1(3)
Axial compression				
β _a (10 ³ GPa ⁻¹)	1.80	1.00(2)		
β _c	0.90	3.30(2)		
Site bulk moduli (GPa)				
M-site	220			
Reference	Hazen and Finger (1981)	Arlt et al. (2000)	Arlt et al. (2000)	Arlt et al. (2000)

* Indicates fixed parameter

Values in brackets give alternative fitting

Table 9. Linear thermal expansion coefficients for rutile-type structures and other TiO₂ polymorphs.

mineral name	stishovite	stishovite	rutile	rutile	brookite	anatase
Formula	SiO ₂	SiO ₂	TiO ₂	TiO ₂	TiO ₂	TiO ₂
space group	P4 ₂ /mmm	P4 ₂ /mmm	P4 ₂ /mmm	P4 ₂ /mmm	Pbca	I4 ₁ /amd
Sample	synthetic	synthetic	synthetic	synthetic	natural	natural
T range	291-873 K	291-773 K	298-1873 K	298-1173 K	298-898 K	298-1073 K
linear thermal expansion coefficients						
α _a (10 ⁻⁶ K ⁻¹)	7.5(2)	8.0	8.9(1)	7.5	6.7	6.6
α _b (10 ⁻⁶ K ⁻¹)					7.0	
α _c (10 ⁻⁶ K ⁻¹)	3.8(3)	2.7	11.1(1)	10.4	10.7	13.5
α _v (10 ⁻⁶ K ⁻¹)	18.6(5)	18.8	29.1(1)	25.5	24.6	27.2
Reference	Endo et al. (1986)	Ito et al. (1974)	Sugiyama and Takéuchi (1991)	Meagher and Lager (1979)	Meagher and Lager (1979)	Horn et al. (1972)

BINARY OXIDES

Introduction

The binary oxide minerals comprise more than a dozen groups of non-silicates containing two different cations. Several of the simpler structures that contain cations in tetrahedral or octahedral coordination have been studied at elevated temperatures or pressures. These structures include minerals of formula ABO_3 (ilmenite and perovskite), AB_2O_4 (spinel, spinelloid, and non-silicate olivines), ABO_4 (scheelite groups), and A_2BO_5 (pseudobrookite group). Of these groups, perovskite is considered in Chapter 14 on framework structures (Ross *this volume*), while olivines and spinelloids are reviewed in Chapter 10 on orthosilicates (Smyth et al. *this volume*).

Binary oxides are of special interest because the presence of two different cations leads to the possibility of varying states of cation order-disorder, which adds complexity to any study of these phases at elevated temperatures and pressures.

Ilmenite Group (ABO_3)

The ilmenite group comprises ilmenite ($FeTiO_3$), geikielite ($MgTiO_3$), pyrophanite ($MnTiO_3$), melanostibite ($Mn(Fe^{3+}, Sb^{5+})O_3$), brizite ($NaSbO_3$) and an as yet unnamed high-pressure polymorph of $MgSiO_3$ (**akimotoite?**). Synthetic compounds with the ilmenite structure also include $CoTiO_3$, $CdTiO_3$, $MnGeO_3$, $MgGeO_3$, and $ZnSiO_3$. The trigonal structure (space group $R\bar{3}$), illustrated in Figure 12, is an ordered derivative of the corundum structure with two distinct cation sites, both in octahedral coordination. The structure is relatively dense, having face-sharing octahedra as in corundum.

The crystal structure of a pure synthetic ilmenite ($FeTiO_3$) was refined at several temperatures to 1050°C and at several pressures to 4.61 GPa by Wechsler and Prewitt (1984). Thermal expansion is nearly isotropic with a linear volumetric thermal expansion coefficient of $30 \times 10^{-6} K^{-1}$ and linear axial expansions of 10.1 and $9.6 \times 10^{-6} K^{-1}$ on a and c respectively. As expected from bond strength considerations, the FeO_6 octahedron is more expansive with a volumetric thermal expansion coefficient of $38 \times 10^{-6} K^{-1}$ compared to $23 \times 10^{-6} K^{-1}$ for the TiO_6 octahedron. These values are larger than, but comparable to, the polyhedral expansion coefficients predicted by equation 1: 36 and $18 \times 10^{-6} K^{-1}$ for Fe and Ti octahedra, respectively. The thermal expansion coefficient of the portion of the unit-cell volume not included in coordination polyhedra (NPV) is $29 \times 10^{-6} K^{-1}$. This value, intermediate between that of Ti and Fe octahedra, reflects the constraints that the rigid linkages of octahedra impose on the structure.

The structure is relatively incompressible, with a bulk modulus of 170 ± 7 GPa and refined $K' = 8 \pm 4$. In contrast to thermal expansion, compression is anisotropic with a and c axes having linear compressibilities of 1.34 and $2.63 \times 10^{-3} GPa^{-1}$, respectively. The bulk modulus of the FeO_6 octahedron is about 140 ± 10 , whereas that of the TiO_6 octahedron is 290 ± 50 GPa. Mean Fe-O and Ti-O bond distances are 2.14 and 1.98 Å, respectively, so equation 3 predicts polyhedral bulk moduli of 153 and 306 GPa, respectively.

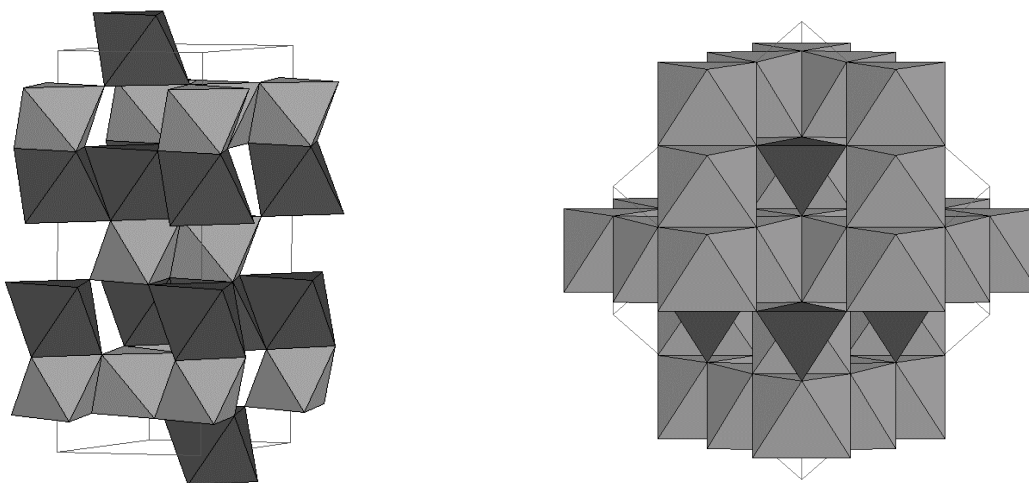


Figure 12. (left) The crystal structure of ilmenite ($FeTiO_3$), c -vertical. The structure is an ordered derivative of the corundum structure (Fig. 4) and is trigonal ($R\bar{3}$) with alternating layers of Fe and Ti octahedra.

Figure 13. (right) The crystal structure of spinel ($MgAl_2O_4$) in approximately (111) projection. The structure is cubic ($Fd\bar{3}m$) with Mg in tetrahedral and Al in octahedral coordination. The inverse spinel structure has Al in tetrahedral coordination with the octahedral site half Mg and half Al.

Spinel Group, AB_2O_4

The spinel group comprises a large number of binary oxide minerals. The principal named end-members include spinel ($MgAl_2O_4$), galaxite ($MnAl_2O_4$), hercynite ($FeAl_2O_4$), gahnite ($ZnAl_2O_4$), magnesioferrite ($MgFe_2O_4$), jacobsonite ($MnFe_2O_4$), magnetite ($FeFe_2O_4$), franklinite ($ZnFe_2O_4$), trevorite ($NiFe_2O_4$), cuprospinel ($CuFe_2O_4$), magnesiochromite ($MgCr_2O_4$), chromite ($FeCr_2O_4$), zincchromite ($MgFe_2O_4$), and ulvospinel ($TiFe_2O_4$). The high-pressure silicate spinels, including ringwoodite (Mg_2SiO_4), are also members of this diverse group, but are discussed in Chapter 10 on orthosilicates (Smyth et al. *this volume*). The spinel structure (Figure 13) is cubic ($Fd\bar{3}m$) with the tetrahedral cation at $(\frac{1}{8}, \frac{1}{8}, \frac{1}{8})$ and the octahedral cation at $(\frac{1}{2}, \frac{1}{2}, \frac{1}{2})$. The oxygen is at (u, u, u) where $u \sim 0.25$, so that the single positional parameter plus the cell edge are sufficient to determine nearest neighbor distances. Hill et al (1979) and O'Neill and Navrotsky (1983) summarized the variation in structure parameters with composition.

Several nonsilicate spinel structures have been studied at elevated temperatures. The mineral spinel, $MgAl_2O_4$, is of special interest because it undergoes a rapid, reversible transition to a disordered state between 600 and 700°C. Its high-temperature structure has been reported by Yamanaka et al. (1983) and Redfern et al. (1999). Harrison et al. (1998) studied the hercynite structure to 1150°C and report a volumetric thermal expansion of $28 \times 10^{-6} \text{ K}^{-1}$.

At pressure, Finger et al. (1986) have studied the structure of spinel ($MgAl_2O_4$) and magnetite to 4.0 and 4.5 GPa, respectively. They report bulk moduli of 194 ± 6 for spinel and 186 ± 5 GPa for magnetite. In good agreement with this study, Nakagiri et al. (1986) report the structure of magnetite to 4.5 GPa and find a bulk modulus of 181 ± 2 GPa. These results are summarized in Table 10.

The behavior of the spinel structure at non-ambient conditions is especially amenable to theoretical treatment. Hazen and Yang (1999) demonstrated that the structural simplicity of the spinel structure allows an exact prediction of bulk modulus and thermal expansivity from knowledge of bond distance variations. In particular, they define structural variations in terms of the tetrahedral and octahedral cation-oxygen distances, d_T and d_O , so that the unit cell parameter, a , is given by the expression:

$$a = \frac{40d_T + 8\sqrt{33d_O^2 - 8d_T^2}}{11\sqrt{3}}$$

or,

$$a = \frac{8}{11\sqrt{3}}(5d_T + A), \quad (\text{equation 4})$$

where:

$$A = \sqrt{33d_O^2 - 8d_T^2}.$$

Changes in cation-oxygen bond distances, for example with temperature or pressure, will therefore lead to predictable variations in unit-cell dimensions. Thus, a 1% increase in d_O results in approximately a 1% change in a , whereas a 1% change in d_T results in approximately a 0.5% change in a .

A more exact expression is derived by differentiating equation 1 with respect to pressure (or temperature):

$$\frac{\partial a}{\partial P} \quad \text{or} \quad \frac{\partial a}{\partial T} = \frac{8}{11\sqrt{3}} \left[5d_T' + \frac{33d_O d_O' - 8d_T d_T'}{A} \right]$$

Dividing this equation by the unit-cell edge a (equation 1 above) yields an exact expression for the linear compressibility (or thermal expansion) of a in terms of bond distances, d_T and d_O , and bond compressibilities (or thermal expansivities):

$$\begin{aligned} -\beta &= \frac{\partial a}{a \partial P} \\ &= \frac{5d_T'}{5d_T + A} + \frac{33d_O d_O' - 8d_T d_T'}{(5d_T + A)A} \quad (\text{equation 5}) \\ \alpha &= \frac{\partial a}{a \partial T} \end{aligned}$$

Cation-anion bond distances, d_T and d_O , are typically known to $\pm 1\%$ from spinel refinements and from tabulations of bond distances. Approximate values of the derivatives of d_T and d_O with respect to pressure and temperature, d_T' and

d_o' , are constrained by high-pressure or high-temperature structure studies, as reviewed in this volume, or from comparative crystal chemical systematics (see Hazen and Prewitt *this volume*).

By employing this relationship, Hazen and Yang (1999) demonstrated that the state of cation order-disorder may have a dramatic effect on spinel bulk modulus or thermal expansion. Compressibilities for normal (fully ordered) versus inverse (with disordered octahedral cations) variants were shown to differ by as much as 17%, while thermal expansivities may differ by as much as 15%.

Pseudobrookite group, A_2BO_5

The pseudobrookite group includes pseudobrookite (Fe_2TiO_5), ferropseudobrookite ($FeTi_2O_5$), karoosite ($MgTi_2O_5$) and armalcolite ($Mg_{0.5}Fe_{0.5}Ti_2O_5$), as well as several synthetic compounds, notably Al_2TiO_5 . The structure, illustrated in Figure 14, is orthorhombic (space group $Bbmm$). There are two octahedral sites, one with point symmetry mm (M1), which is larger and more distorted, and the other with point symmetry m (M2). At low temperatures, karoosite, armalcolite and ferropseudobrookite are ordered, with the divalent cation in M1 and the tetravalent cation in M2. Morosin and Lynch (1972) investigated the structure of Al_2TiO_5 up to 600°C and Wechsler (1977) investigated the structure of armalcolite to 1100°C. Wechsler (1977) observed a volumetric thermal expansion of $32 \times 10^{-6} K^{-1}$ over this temperature range. The structure at high temperature was disordered, whereas annealing at 400°C produced an ordered structure at low temperature. Bayer (1971) reported the cell expansion of karoosite and observed moderate expansion anisotropy with $\alpha_b > \alpha_a > \alpha_c$.

Hazen and Yang (1997) synthesized karoosite single crystals with a range of ordered states, and found that the bulk modulus varies by as much as 6%, based on the distribution of Ti and Mg between the two octahedral positions. Subsequent structural studies at room pressure (Yang and Hazen 1998) and high pressures to 7.5 GPa (Yang and Hazen 1999) revealed the underlying structural causes for this variation. In all structures, TiO_6 octahedra (octahedral bulk modulus = 250 GPa) are observed to be much less compressible than MgO_6 octahedra (octahedral bulk modulus = 170 GPa). Disordered octahedra with intermediate Mg-Ti occupancies, furthermore, display intermediate bulk moduli.

The pseudobrookite structure (figure 14) consists of layers of M2 octahedra that share edges in the (010) plane. Thus, both a - and c -axis compressibilities are dictated almost exclusively by the compression of M2. If M2 is fully occupied by Ti, as in ordered karoosite, then a - and c -axis compressibility will be minimized. In disordered karoosite, on the other hand, M2 compressibility will be greater in proportion to Mg/Ti, and both a and c axes will respond accordingly. The b -axis compression, on the other hand, always represents an average of M1 + 2M2, so its compressibility is unaffected by cation disorder.

Scheelite group, ABO_4

The scheelite-group oxide minerals include scheelite ($CaWO_4$), powellite ($CaMoO_4$), stolzite ($PbWO_4$), and wulfenite ($PbMoO_4$). The scheelite structure is rather versatile in that it can accommodate +1, +2, +3 and +4 A cations with +7, +6, +5, and +4 tetrahedral B cations, respectively. In this way, many synthetic compounds occur with this structure, including, $SrWO_4$, $BiVO_3$, $LaNbO_4$, for example. The structure of scheelite, illustrated in Figure 15, is tetragonal ($I4_1/a$) with two symmetrically distinct cations and one oxygen atom in a general position: Ca at (0, 1/4, 5/8), W at (0, 1/4, 1/8), and oxygen at approximately (0.15, 0.01, 0.21). The ^{VIII}Ca site is edge-sharing with four nearest ^{VIII}Ca sites and corner-sharing with eight nearest tetrahedral sites. Each tetrahedron is connected to eight ^{VIII}Ca sites, because every oxygen atom is coordinated to two Ca positions. The structures of pure synthetic scheelite and powellite were refined at several pressures to 4.1 and 6.2 GPa, respectively, by Hazen et al. (1985). In addition, Hazen et al. measured unit cell parameters of stolzite, wulfenite and $CdMoO_4$ at several pressures to about 5 GPa. Their results are summarized in Table 11. There are as yet no refinements of these structures at elevated temperatures.

The scheelite-type structures are relatively compressible, with bulk moduli ranging from about 64 GPa for wulfenite and stolzite to a maximum of 104 GPa for $CdMoO_4$. The axial compression is anisotropic for the five scheelite-type structures investigated, with c/a decreasing upon compression. Little or no volume change was observed in the W and Mo tetrahedra, with bulk moduli of these rigid +6 cation polyhedra being in excess of 500 GPa. Most of the compression is taken up by the divalent 8-coordinated polyhedron and the non-polyhedral volume. Differences in the bulk moduli of different scheelite-type minerals and compounds thus result mainly from the difference in size and valence of eight-coordinated cations. Polyhedral compressibility is typically proportional to the polyhedral volume divided by the cation charge, so that the most compressible structural units tend to be large polyhedra with cations of low valence. Therefore, it is expected that the most compressible tungstates and molybdates should be of the form $A^{1+}B^{7+}O_4$, with +1 cations in eight coordination and +7 cations in tetrahedral coordination. The least compressible scheelite-type compounds, on the other hand, would then be expected for $A^{4+}B^{4+}O_4$ such as $ZrGeO_4$.

Table 10. Comparative crystal chemistry of binary oxides.

Structure	phase formula	CN ^{cation}	Pmax (GPa)	compression		Ref.	expansion		Ref.	
				K _{T0} (GPa)	∂K/∂P		T-range (K)	α _V (10 ⁻⁶ K ⁻¹)		
spinel	MgAl ₂ O ₄	spinel (norm)	4.0	194(6)	4*	[1]	293-873	28.6 [†]	[2]	
				120(20)	4*		293-873	35.5 [†]		
				260(40)	4*		293-873	23.7 [†]		
	FeAl ₂ O ₄	hercynite	4.5	186(5)	190(20)	4*	[1]	298-973	25.2 ^{††}	[3]
					190(20)	4*		298-973	24.0 ^{††}	
FeFe ₂ O ₄	magnetite	4.5	186(5)	190(20)	4*	[1]	293-843	20.6	[4]	
ilmenite	FeTiO ₃	ilmenite	4.6	177(3)	4*	[5]	297-1323	30.2	[5]	
				140(10)	4*		297-1323	38.0		
				289(64)	4*		297-1323	23.1		
perovskite	CaTiO ₃	perovskite	10.4	210(7)	5.6*	[6]				
	MgSiO ₃	silicate perov.	12.6	254(13)	4*	[7]	298-381	22(8)	[8]	
				333	4*					
				244	4*					
pseudobrookite	(Fe,Mg)Ti ₂ O ₅	armalcolite					297-1373	44.6	[9]	
	MgTi ₂ O ₅	karrooite (ordered)	7.5	165(1)	4*	[10]			[11]	
				172(4)						
					250(7)					
	MgTi ₂ O ₅	karrooite (disordered)	7.5	158(1)	214(18)	4*	[10]			
237(13)										
sheelite	CaWO ₄	sheelite	4.1	68(9)	4*	[12]				
	PbWO ₄	wulfenite		71						
	CaMoO ₄	powellite	4.1	64(2)	4*	[12]				
				81.5(7)	4*					
					67					
	PbMoO ₄	stolzite	5.3	64(2)	4*	[12]				
CdMoO ₄		4.8	104(2)	4*	[12]					

*Indicates fixed parameter.

[†]Inversion character is < 1% over the temperature range used in the calculation of volume expansion.^{††}Inversion character is 13% at end points; room temperature and 973 K.

References: [1] Finger et al. (1986) [7] Ross and Hazen (1990)
[2] Yamanaka and Takéuchi (1983) [8] Ross and Hazen (1989)
[3] Harrison et al. (1998) [9] Wechsler (1977)
[4] Skinner (1966) [10] Yang and Hazen (1999)
[5] Wechsler and Prewitt (1984) [11] Bayer (1971)
[6] Xiong et al. (1986) [12] Hazen et al. (1985)

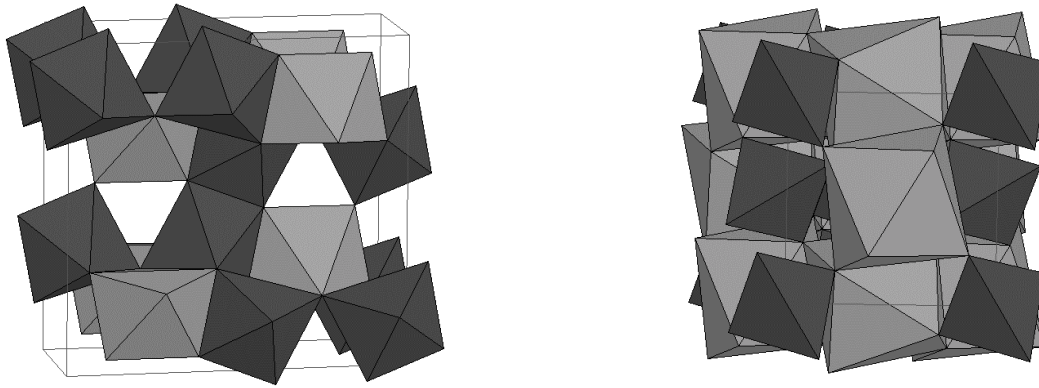


Figure 14. (left) The crystal structure of pseudobrookite (Fe_2TiO_5). The structure is orthorhombic ($Bbmm$) with two distinct octahedral sites. M1 (light shading) has point symmetry mm and M2 (dark) has point symmetry m .

Figure 15. (right) The crystal structure of scheelite (CaWO_4). The structure is tetragonal ($I4_1/a$) with W in tetrahedral coordination and Ca in eight-fold coordination.

Table 11. Compression of scheelite-type tungstates and molybdates.

mineral name	sheelite	wulfenite	powellite	stolzite	
Formula	CaWO_4	PbWO_4	CaMoO_4	PbMoO_4	CdMoO_4
Sample	synthetic	synthetic	synthetic	synthetic	synthetic
Pmax (GPa)	4.1	6.0	6.2	5.3	4.8
K_{T0} (GPa)	68(9)	64(2) [38(2)]	81.5(7) [88(2)]	64(2) [57(5)]	104(2) [117(4)]
K'	[61(10)]	4* [23(2)]	4* [2(1)]	4* [8(3)]	4* [-2(2)]
Axial compression					
β_a (10^{-3} GPa^{-1})	3.87	3.05	3.04	3.48	2.56
β_c	4.98	6.15	4.48	6.41	3.73
Site bulk moduli (GPa)					
T-site (^{IV}W and ^{IV}Mo)	>500		>500		
^{VIII}Ca	71		67		
Reference	Hazen et al. (1985)				

*Indicates fixed parameter.

[Values in brackets indicate alternate fitting]

FUTURE OPPORTUNITIES

Despite the extensive literature on the structural response of oxide minerals to temperature and pressure, numerous opportunities remain for future research. These opportunities include both experimental and theoretical challenges.

- **Other Phases:** The structures of many important oxide minerals have not been investigated at temperature or pressure. Among the single oxides are cuprite (Cu_2O), zincite (ZnO), litharge and massicot (PbO), romarchite (SnO), montroydite (HgO), Ti_2O_3 , bixbyite (Mn_2O_3), senarmontite and valentinite (Sb_2O_3), arsenolite and claudetite (As_2O_3), bismite (Bi_2O_3), pyrolusite (MnO_2) and baddeleyite (ZrO_2).

A large number of binary oxide structures also remain to be investigated at non-ambient conditions. These compounds include dozens of phases with the ilmenite, spinel, pseudobrookite and scheelite structures: systematic structural investigations of each of these groups would be welcome. In addition, numerous other non-mineral structure types that were not discussed here offer the opportunity to explore unusual structural geometries, coordination polyhedra, and cations that are inherently non-spherical. To cite just one example, the structure of $\text{Ca}_4\text{Bi}_6\text{O}_{13}$ (Parise et al. 1990) features both three-coordinated pyramidal and five-coordinated pyramidal arrangements of oxygen around Bi atoms – “polyhedra” in which the cation’s lone pair of electrons acts as a fourth (tetrahedral) and sixth (octahedral) anion, respectively. High-pressure structures of this phase (and any of the numerous related alkaline earth-bismuth oxides) would complement the existing literature, which focuses primarily on more conventional structure types.

Other opportunities are provided by comparisons among isostructural – but not isoelectronic – compounds, such as the 1+/7+ scheelites versus the 4+/4+ scheelites. These isomorphous suites can provide special insight into the origins of structural variations with temperature and pressure. The 2+/4+ versus 3+/2+ spinels are another example of special interest to geophysical modeling.

In addition to continuous structural variations with temperature and pressure, many of these compounds display phase transitions that should be documented more thoroughly with crystallographic techniques.

- **Studies at Pressures > 10 GPa:** Most previous studies of oxides, including bromellite, corundum-type, rutile-type, spinel-type and scheelite-type compounds, were completed more than a decade ago, before the improvements in pressure cells, data collection techniques, and analysis procedures described in this volume. All of these structural studies could be profitably revisited. Such high-pressure refinements could, for example, shed light on the role of polyhedral distortions (i.e., O-M-O bond bending) in crystal compression. Such studies might also reveal structural mechanisms that lead to values of K' that differ significantly from 4. Why, for example, does rutile have $K' \sim 7$? In a perhaps related question, what is the role of cation-cation repulsion in the high-pressure behavior of minerals? Refinements of improved precision at $P > 10$ GPa should reveal such details of structural variation not previously available.
- **Combined Pressure-Temperature Studies:** Precise and accurate structure studies of oxide minerals at simultaneous high temperature and pressure offer the best opportunity for comprehensive structural equations of state. Though technically challenging, these studies would provide great insight into the behavior of minerals in geologically relevant environments.

Of special interest in this regard are studies of binary oxides that can undergo order-disorder reactions. Quench experiments only hint at the complex interplay among equation-of-state parameters, cation ordering, and structural variations with temperature and pressure (Hazen and Navrotsky 1996). *In situ* investigation of spinel-type MgAl_2O_4 (Hazen and Yang 1999) or pseudobrookite-type MgTi_2O_5 (Yang and Hazen 1999), for example, might elucidate this behavior.

REFERENCES

- Adams DM, Christy AG, Haines J, and Clark SM (1992) Second-order phase transition in PbO and SnO at high pressures: Implications for the litharge-massicot phase transformation. *Phys Rev B* 46:11358-11367
- Akaogi M, Kusaba K, Susaki J-I, Yagi T, Matsui M, Kikegawa T, Yusa H, Ito E (1992) High-pressure high-temperature stability of αPbO_2 -type TiO_2 and MgSiO_3 majorite: calorimetric and in situ X-ray diffraction studies. *In: High-pressure research: Application to Earth and Planetary Sciences*. Syono Y, Manghnani MH (eds) 447-455
- Aldebert P, Traverse, JP (1984) A high-temperature thermal expansion standard. *High Temp-High Press* 16:127-135
- Anderson DL and Anderson OL (1970) The bulk modulus-volume relationship for oxides. *J Geophys Res* 75:3494-3500
- Anderson OL and Nafe JE (1965) The bulk modulus-volume relationship for oxide compounds and related geophysical problems. *J Geophys Res* 70:3951-3963
- Angel RJ, Allan DR, Miletich R, Finger LW (1997) The use of quartz as an internal pressure standard in high-pressure crystallography. *J Appl Cryst* 30:461-466

- Arlt T, Bermejo M, Blanco MA, Gerward L, Jiang JZ, Olsen JS, Recio JM (2000) High-pressure polymorphs of Anatase TiO₂ *submitted*
- Aurivillius K (1956) The crystal structure of mercury (II) oxide Acta Cryst 9:685-686
- Bayer G (1971) Thermal expansion and stability of pseudobrookite-type compounds, Me₃O₅. J Less Common Metals, 24:129-138
- Benjamin TM, Zou G, Mao HK, Bell PM (1981) Equations of state for thorium metal, UO₂, and a high-pressure phase of UO₂ to 650 kbar. Carnegie Inst Wash Yearb 80:280-283
- Bragg L, Claringbull GF, Taylor WH (1965) *Crystal Structures of Minerals*. Cornell Univ Press, Ithaca, 409pp
- Clendenen RL, Drickamer HG (1966) Lattice parameters of nine oxides and sulfides as a function of pressure. J Chem Phys 44:4223-4228
- d'Amour H, Schiferl D, Denner W, Schulz H, Holzapfel WB (1978) High-pressure single-crystal structure determinations for ruby up to 90 kbar using an automated diffractometer. J Appl Phys 49:4411-4416
- Drickamer HG, Lynch RW, Clendenen RL, Perez-Albuera EA (1966) X-ray diffraction studies of the lattice parameters of solids under very high pressure. Sol State Phys 19:135-229
- Duffy TS, Hemley RJ, Mao H-k (1995) Equation of state and shear strength at multimegabar pressures: Magnesium oxide to 227 GPa. Phys Rev Lett 74:1371-1374
- Endo S, Akai T, Akahama Y, Wakatsuki M, Nakamura T, Tomii Y, Koto, K, Ito, Y (1986) High temperature X-ray study of single crystal stishovite synthesized with Li₂WO₄ as flux. Phys Chem Minerals 13:146-151
- Fei Y (1999) Effects of temperature and composition on the bulk modulus of (Mg,Fe)O Am Mineral 84:272-276
- Fei Y, Frost DJ, Mao HK, Prewitt CT, Häusermann D (1999) In situ structure determination of the high pressure phase of Fe₃O₄. Am Mineral 84:203-206
- Finger LW, Hazen RM (1978) Crystal structure and compression of ruby to 46 kbar. J Appl Phys, 49:5823-5826
- Finger LW, Hazen RM (1980) Crystal structure and isothermal compression of Fe₂O₃, Cr₂O₃, and V₂O₃ to 50 kbars. J Appl Phys 51:5362-5367
- Finger LW, Hazen RM, Hofmeister AM (1986) High-pressure crystal chemistry of spinel (MgAl₂O₄) and magnetite (Fe₃O₄): comparisons with silicate spinels. Phys Chem Minerals 13:215-220
- Fritz IJ (1974) Pressure and temperature dependences of the elastic properties of rutile (TiO₂) J Phys Chem Solids 35:817-826
- Harrison RJ, Redfern SAT, O'Neill HSC (1998) The temperature dependence of the cation distribution in synthetic hercynite (FeAl₂O₄) from in-situ neutron structure refinements. Am Mineral 83:1092-1099
- Hazen RM (1976) Effects of temperature and pressure on the cell dimension and X-ray temperature factors of periclase. Am Mineral 61:266-271
- Hazen RM (1981) Systematic variation of bulk modulus of wüstite with stoichiometry. Carnegie Inst Wash Yearb 80:277-280
- Hazen RM and Finger LW (1977) Crystal structure and compression of ruby to 80 kbar. Carnegie Inst Wash Yearb 76:525-527
- Hazen RM and Finger LW (1979a) Bulk modulus-volume relationship for cation-anion polyhedra. J Geophys Res 84:6723-6728
- Hazen RM and Finger LW (1979b) Studies in high-pressure crystallography. Carnegie Inst Wash Yearb 78:632-635
- Hazen RM, Finger LW (1981) Bulk moduli and high-pressure crystal structures of rutile-type compounds. J Phys Chem Solids 42:143-151
- Hazen RM, Finger LW (1982) *Comparative Crystal Chemistry*. Wiley, New York, 231 p
- Hazen RM, Finger LW (1986) High-pressure and high-temperature crystal chemistry of beryllium oxide J Appl Phys 59:728-733
- Hazen RM Jeanloz R (1984) Wüstite (Fe_{1-x}O): A review of its defect structure and physical properties. Rev Geophys Space Phys 22:37-46
- Hazen RM, Prewitt, CT (1977) Effects of temperature and pressure on interatomic distances in oxygen-based minerals, Am Mineral 62: 309-315
- Hazen RM, Yang H (1997) Cation disorder increases compressibility of pseudobrookite-type MgTi₂O₅. Science 277:1965-1967
- Hazen RM, Yang H (1999) Effects of cation substitution and order disorder on P-V-T equations of state of cubic spinels. Am Mineral 84:1956-1960
- Hazen RM Finger LW Mariathasan JWE (1985) High-pressure crystal chemistry of scheelite-type tungstates and molybdates. J Phys Chem Solids 46:253-263
- Heinz DL, Jeanloz R (1984) Compression of the B2 high-pressure phase of NaCl. Phys Rev B 30:6045-6050
- Hill RJ, Craig JR, Gibbs GV (1979) Systematics of the spinel structure type. Phys Chem Mineral, 4:317-339
- Horn M, Schwerdtfeger CF, and Meagher EP (1972) Refinement of the structure of anatase at several temperatures Zeit Krist 136:273-281
- Huang E, Kaoshung J, Cheng YS (1994) Bulk modulus of NiO. J Geol Soc China 37:7-16
- Irifune T, Fujino K, Ohtani E (1991) A new high pressure form of MgAl₂O₄. Nature 349:409-411
- Ito H, Kawada K, Akimoto S-I (1974) Thermal expansion of stishovite. Phys Earth Planet Int 8: 277-281
- Jacobsen SD, Angel RJ, Reichmann H-J, Mackwell SJ, McCammon CA, Smyth JR, and Spetzler HA (1999) Hydrostatic compression of single-crystal magnesio-wüstite. EOS Transactions 80:937
- Jamieson JC (1970) The phase behavior of simple compounds. Phys Earth Planet Int 3:201-203

- Jayaraman A (1972) Pressure-induced electronic collapse and semiconductor-to-metal transition in EuO. *Phys Rev Lett* 29:1674-1676
- Jayaraman A, Batlogg B, Maines RG, Bach H (1982) Effective ionic charge and bulk modulus scaling in rock-salt structured rare-earth compounds. *Phys Rev B* 26: 3347-3351
- Jeanloz R, Hazen RM (1983) Compression, nonstoichiometry, and bulk viscosity of wüstite. *Nature* 304: 620-622
- Jeanloz R, Rudy A (1987) Static compression of MnO manganosite to 60 GPa. *J Geophys Res* 92:11,433-11,436
- Jeanloz R, Sato-Sorensen Y (1986) Hydrostatic compression of Fe_{1-x}O wüstite. *J Geophys Res* 91:4665-4672
- Jeanloz R, Ahrens TJ, Mao HK, Bell PM (1979) B1-B2 transition in calcium oxide from shock-wave and diamond-cell experiments. *Science* 206:829-830
- Kudoh Y, Takeda H (1986) Single crystal X-ray diffraction study on the bond compressibility of fayalite, Fe₂SiO₄ and rutile, TiO₂ under high pressure. *Physica B* 139-140:333-336
- Kudoh Y, Takeda H, Arashi H (1986) In situ determination of crystal structure for high pressure phase of ZrO₂ using a diamond anvil and single crystal X-ray diffraction method. *Phys Chem Minerals* 13: 233-237
- Leger JM, Tomaszewski PE, Atouf A, Pereira, AS (1993a) Pressure-induced structural phase transitions in zirconia under high pressure. *Physical Review B* 47:14075-14083
- Leger JM, Atouf A, Tomaszewski PE, Pereira AS (1993b) Pressure-induced phase transitions and volume changes in HfO₂ up to 50 GPa. *Physical Review B* 48:93-98
- Liu L-G (1971) A dense modification of BaO and its crystal structure. *J Appl Phys* 42:3702-3704
- Liu L-G (1977) The post-spinel phase of twelve silicates and germanates. *In: High-pressure research: Applications in geophysics*. Manghnani MH, Akimoto S (eds) Academic Press, New York 245-253
- Liu L-G, Bassett WA (1986) Elements, Oxides, and Silicates: High-pressure phases with implications for the Earth's interior. Oxford University Press, New York pp 250
- Liu L-G, Bassett WA (1973) Changes in the crystal structure and the lattice parameter of SrO at high pressure. *J Geophys Res* 78:8470-8473
- Manghnani M (1969) Elastic constants of single-crystal rutile under pressures to 7.5 kilobars. *J Geophys Res* 74:4317-4328
- Mao H-K, Shu J, Fei Y, Hu J, Hemley RJ (1996) The wüstite enigma, *Phys Earth Planet Int*, 96:135-145
- McWhan DB, Remeika JP (1970) Metal-insulator transition in (V_{1-x}Cr_x)₂O₃. *Phys Rev B* 2:3734-3750
- Meagher EP, and Lager GA (1979) Polyhedral thermal expansion in the TiO₂ polymorphs: Refinement of the crystal structures of rutile and brookite at high temperature. *Can Mineral* 17:77-85
- Minomura S, Drickamer HG (1963) Effect of pressure on the electrical resistance of some transition-metal oxides and sulfides. *J Appl Phys* 34:3043-3048
- Morosin B, Lynch RW (1972) Structure studies on Al₂TiO₅ at room temperature and at 600°C. *Acta Cryst B*28:1040-1046
- Nakagiri N, Manghnani M, Ming LC, Kimura S (1986) Crystal structure of magnetite under pressure. *Phys Chem Minerals* 13:238-244
- Noguchi Y, Kusaba K, Fukuoka K, Syono Y (1996) Shock-induced phase transition of MnO around 90 GPa. *Geophys Res Lett* 23:1469-1472
- O'Neill HS, Navrotsky A (1983) Simple spinels: crystallographic parameters, cation radii, lattice energies, and cation distribution. *Am Mineral* 68:181-194
- Parise JB, Torardi CC, Whangbo MH, Rawn CJ, Roth RS, Burton BP (1990) Ca₄Bi₆O₁₃, a compound containing an unusually low bismuth coordination and short Bi-Bi contacts. *Chemistry of Materials* 2:454-458
- Redfern SAT, Harrison RJ, O'Neill H.St.C, Wood DRR (Thermodynamics and kinetics of cation ordering in MgAl₂O₄ spinel up to 1600°C from in situ neutron diffraction. *Am Mineral* 84:299-310
- Reichmann H-J, Jacobsen SD, Mackwell SJ, McCammon CA (2000) Sound wave velocities and elastic constants for magnesiowüstite using gigahertz interferometry. *Geophys Res Lett* 27: *in press*
- Rice CE, Robinson WR (1977) High-temperature crystal chemistry of Ti₂O₃: Structural changes accompanying the semiconductor-metal transition. *Acta Cryst B*33:1342-1348
- Richet P, Mao HK, Bell PM (1988) Static compression and equation of state of CaO to 135 Mbar *J Geophys Res* 93:15279-15288
- Richet P, Xu J-A, Mao H-K (1988) Quasi-hydrostatic compression of ruby to 500 kbar *Phys Chem Minerals* 16:207-211
- Robinson WR (1975) High temperature crystal chemistry of V₂O₃ and 1% chromium-doped V₂O₃. *Acta Cryst*, B31:1153-1160
- Ross NL, Hazen RM (1989) Single crystal X-ray diffraction study of MgSiO₃ perovskite from 77 to 400 K. *Phys Chem Min* 16:415-420
- Ross NL, Hazen RM (1990) High-pressure crystal chemistry of MgSiO₃ perovskite. *Phys Chem Min* 17:228-237
- Ross NL, Shu JF, Hazen RM, Gasparik T (1990) High-pressure crystal chemistry of stishovite. *Am Mineral* 75:739-747
- Samara GA, Peercy PS (1973) Pressure and temperature dependence of the static dielectric constants and Raman spectra of TiO₂ (rutile). *Phys. Rev. B*7, 1131-1148.
- Sato Y, Jeanloz R (1981) Phase transition in SrO. *J Geophys Res* 86:11773-11778
- Sirdeshmukh DB Subhadra KG (1986) Bulk modulus-volume relationship for some crystals with a rock salt structure. *J Appl Phys* 59:276-277

- Sato Y, Akimoto S (1979) Hydrostatic compression of four corundum-type compounds: α -Al₂O₃, V₂O₃, Cr₂O₃, and α -Fe₂O₃. *J Appl Phys* 50:5285-5291
- Simmons G, Wang H (1971) *Single Crystal Elastic Constants*. MIT Press, Cambridge MA
- Simons PY, Datchile F (1967) The structure of TiO₂ II, a high pressure phase of TiO₂. *Acta Cryst* 23:334-336
- Skinner BJ (1966) Thermal expansion. *In: Handbook of Physical Constants*. Clark SP (ed) Jr Geol Soc Amer Mem pp 75-95
- Sugiyama K, Takéuchi, Y (1991) The crystal structure of rutile as a function of temperature up to 1600°C. *Zeit Krist* 194:305-313
- Sugiyama M, Endo S, Koto K (1987) The crystal structure of stishovite under pressure up to 6 GPa. *Mineral J* 13:455-466
- Suzuki I, Okajima S, Seya K (1979) Thermal expansion of single-crystal manganosite. *J Phys Earth* 27:63-69
- Touloukian YS, Kirby RK, Taylor RE, Desai PD (1977) Thermal expansion: Nonmetallic solids. *In: Thermophysical Properties of Matter*. Touloukian YS, Ho CY (eds) Plenum, New York, 13, 176pp
- Wechsler BA (1977) Cation distribution and high temperature crystal chemistry of armakolite. *Am Mineral* 62:913-920
- Wechsler BA, Prewitt CT (1984) Crystal structure of ilmenite at high temperature and high pressure *Am Mineral* 69:176-185
- Werner A, Hochheimer HD (1982) High-pressure X-ray study of Cu₂O and Ag₂O. *Phys Rev B* 25:5929-5934
- Wier ST, Vohra YK, Ruoff AL (1986) High-pressure phase transitions and the equations of state of BaS and BaO. *Phys Rev B* 33:4221-4226
- Winslow GH (1971) Thermal mechanical properties of real materials: The thermal expansion of UO₂ and ThO₂. *High Temp Sci* 3:361-367
- Xiong DH, Ming LC, Manghnani MH (1986) High pressure phase transformations and isothermal compression in CaTiO₃ (perovskite). *Phys Earth Planet Int* 43:244-252
- Yagi T, Suzuki T, Akimoto S (1985) Static compression of wüstite (Fe_{0.98}O) to 120 GPa. *J Geophys Res* 90:8784-8788
- Yamanaka T, Takéuchi T (1983) Order-disorder transition in MgAl₂O₄ spinel at high temperatures up to 1700°C *Zeit Krist* 165:65-78
- Yang H, Hazen RM (1998) Crystal chemistry of cation order-disorder in pseudobrookite-type MgTi₂O₅. *J Solid State Chem* 138:238-244
- Yang H, Hazen RM (1999) Comparative high pressure crystal chemistry of karooite (Mg₂TiO₅) with different ordering states. *Am Mineral* 84:130-137
- Zimmer HG, Takemura K, Syassen K, Fischer K (1984) Insulator-metal transition and valence instability in EuO near 130 kbar. *Phys Rev B* 29:2350-2352
- Zhang J (1999) Room-temperature compressibilities of MnO and CdO: further examination of the role of cation type in bulk modulus systematics. *Phys Chem Minerals* 26:644-648

